Journal of Human Evolution 59 (2010) 289–305

Contents lists available at ScienceDirect

Journal of Human Evolution

journal homepage: www.elsevier.com/locate/jhevol

An OSL chronology for the sedimentary deposits from Pinnacle Point Cave 13B—A punctuated presence☆

Zenobia Jacobs

Centre for Archaeological Science, School of Earth and Environmental Sciences, University of Wollongong, Wollongong, NSW 2522, Australia

ARTICLE INFO

Article history:
Received 19 January 2010
Accepted 19 March 2010

Keywords:
Optically Stimulated Luminescence
Middle Stone Age
D_e distribution
Single grains
Dunes
Marine Isotope Stage 5

ABSTRACT

Optically stimulated luminescence (OSL) measurements are reported for single aliquots and single grains of quartz from sedimentary deposits within Cave 13B at Pinnacle Point, South Africa (PP13B). Ages have been obtained for 30 samples from the Middle Stone Age and from sterile geological deposits at the base and top of the sediment sequence. The ages for all the archaeological units have been obtained from single-grain measurements that enable unrepresentative grains to be rejected after they have been scrutinized for their OSL behavior. The shape of the equivalent dose distribution and the degree of spread in equivalent dose for each sample have also been scrutinized for evidence of depositional and post-depositional effects that can influence the accuracy of the age estimates. This study also used the same systematic approach as that used for the dating of the Howieson's Poort and Still Bay in South Africa. This single-grain approach results in more accurate and precise age estimates that place all ages measured and analyzed in this way on a common timescale. Four periods of human occupation have been dated to ~162 ka, ~125 ka, ~110 ka, and ~99–91 ka during Marine Isotope Stage (MIS) 6, 5e, 5d, and 5c, respectively. Occupation of the site appears to have occurred at periods of higher sea level and increased aeolian activity, and the cave was ultimately sealed by the accumulation of a large dune ~90 ka ago that infilled the cave, but also blanketed the cliff face above the cave, thus preventing further habitation of the site until ~39 ka.

Introduction

A common need in archaeology is for objects and events of interest to be dated so that they can be arranged in the correct chronological sequence. To accomplish this degree of chronological resolution requires the application of numerical dating methods. Such methods produce quantitative age estimates that can be positioned on a standard timescale, usually expressed as years before present. Each of these numerical methods has uncertainties (expressed as standard errors at 1σ) that are associated with the various measurements made to determine the numerical age. The age and its uncertainty are of equal significance and should not be separated when archaeological interpretations are made.

A number of different numerical dating methods have been used to obtain age estimates for samples collected from Middle Stone Age (MSA) contexts in Southern Africa: radiocarbon (^{14}C) dating (Bird et al., 2003), optically stimulated luminescence (OSL) dating of sediments (Jacobs et al., 2008a, c), thermoluminescence (TL) dating of sediments (Feathers, 2002) and burnt stones (Tribolo et al., 2006, 2009), electron spin resonance (ESR) dating of teeth (Grün and Beaumont, 2001), uranium series (U-series) dating of speleothems (Vogel, 2001), and amino acid racemization (AAR) dating of ostrich eggshell (Miller et al., 1999). Most of these dating efforts have been directed towards obtaining chronologies for the Still Bay (SB) and Howieson's Poort (HP) cultural phases because of their importance to questions of modern human behavior and dispersals (e.g., Miller et al., 1999; Jacobs and Roberts, 2008, 2009a, b; Jacobs et al., 2008c; Tribolo et al., 2009). There has recently also been increased interest in dating MSA assemblages postdating the HP as it remains an enigma why people abandoned their more elaborate SB and HP toolkits in favor of a more traditional MSA toolkit (e.g., Jacobs et al., 2008a, b).

Jacobs and Roberts (2008) critically reviewed all the published age estimates for the SB and HP industries and the techniques used to generate the ages. They demonstrated the generally poor precision (5–20% at the 68% confidence interval) associated with these ages and the large scatter in age estimates, which they termed the chronological 'haze.' This chronological 'haze' is an inevitable result of different dating methods being applied to different materials by

☆ This article is part of 'The Middle Stone Age at Pinnacle Point Site 13B, a Coastal Cave near Mossel Bay (Western Cape Province, South Africa)' Special Issue.

E-mail address: zenobia@uow.edu.au.

0047-2484/$ – see front matter © 2010 Elsevier Ltd. All rights reserved.
doi:10.1016/j.jhevol.2010.07.010

different operators using different equipment, calibration standards, measurement procedures, and data analysis techniques. The effect of this 'haze' is that it prohibits the detection of any stratigraphic trends, frustrates direct comparisons between artifact assemblages from different sites, prevents determination of the duration of cultural phases and, therefore, limits our capacity to interpret the archaeological record within a context of widespread cultural, demographic, and environmental change.

One way of reducing the chronological 'haze' is to perform a systematic dating study using the same method, operator, equipment, measurement, and analytical procedures for every sample to overcome systematic biases. Jacobs et al. (2008c) demonstrated the power of such an approach when they systematically applied single-grain OSL dating to 28 samples collected from SB and HP contexts from nine sites across Southern Africa and combined the study with statistical modeling. They were able to pinpoint the SB and HP industries with unprecedented accuracy and precision (~3–5% at the 68% confidence interval). Jacobs et al. (2008a, b, c) showed that the SB and HP and the MSA postdating the HP consist of relatively short duration, punctuated occupations and that, at least in caves and rock shelters in Southern Africa, there seems to be a pattern emerging. Without the reproducibility and precision attained in these studies, such patterns will not be clear since the durations of these industries-related occupations are relatively short. The durations are of similar magnitude to the changes observed for styles during the LSA (Jacobs and Roberts, 2008). The advantage of dating the HP and SB is that they represent clearly identifiable marker horizons, and shifts within these relatively short-lived industries are marked not only by time, but supported by changes in technologies and subsistence strategies (e.g., d'Errico and Henshilwood, 2007; Lombard, 2007; Soriano et al., 2007; Clark and Plug, 2008; Wadley, 2008; Wadley and Mohapi, 2008; Villa et al., 2010).

Comparatively little, however, is known about the ages and durations of the industries before the SB. Also, the lithic and faunal assemblages of much of this period demonstrate few diagnostic traits and it is difficult to, on the basis of these records alone, determine whether there are any significant age gaps in excavated sequences at any site and which assemblages from different sites are contemporaneous. Only a small number of samples from MSA sequences prior to the SB have been dated using different dating techniques (e.g., Vogel, 2001; Grün and Beaumont, 2001; Feathers, 2002; Jacobs et al., 2006c; Marean et al., 2007; Jacobs et al., 2008b), but no systematic dating studies have yet been conducted across Southern Africa for this early time period, nor have the archaeological assemblages been compared systematically (see Thompson et al. [2010]). Obtaining ages for this part of the MSA is important as it represents at least half of the currently known duration of the MSA in Southern Africa (~170–22 ka; Opperman and Heydenrych, 1990; Marean et al., 2007). The ideal would be to persist with the systematic approach of Jacobs et al. (2008c) and place all of the Southern African MSA on this common timescale.

In this context, the sequence at Pinnacle Point Cave 13B (PP13B), along the southern Cape coast of South Africa, is of particular interest. It was recently demonstrated that PP13B has preserved MSA assemblages older than the SB that extend back to Marine Isotope Stage (MIS) 6, ~164 ka ago (Marean et al., 2007). Our dating of the PP13B sediments provides the first step towards dating the pre-SB deposits using the systematic approach of Jacobs et al. (2008c) that will place it on a common timescale with those already published ages for the SB, HP, and post-HP (Jacobs et al., 2008a, b, c; Jacobs and Roberts, 2008). The purpose of this paper is to provide the methodological and analytical information underpinning the optical dating results to provide confidence in the derived age estimates. Only when the chronology of the entire MSA has been improved substantially can we hope to understand the underlying controls on modern human evolution and dispersals.

Site background and stratigraphy

PP13B is a large sea cave, located ~15 m above present mean sea level, ~10 km west of the southern Cape coastal town of Mossel Bay, and ~400 km east of Cape Town. Other MSA sites in its vicinity include Nelsons Bay Cave near Plettenberg Bay and further afield towards the east and west of PP13B are the well-known sites of Klasies River, Blombos Cave, and Die Kelders (see Marean et al. [2010: their Fig. 1]). PP13B is about 8 m wide and 30 m deep (Fig. 1) and was eroded into a fault breccia, which represents a shear zone in the Table Mountain Sandstone (TMS) cliff face. The geology of the cave and its configuration has previously been presented in Marean et al. (2007) and is further discussed in Marean et al. (2010). Relatively large areas (13 m^2) of sedimentary deposits have been excavated in PP13B. The main focus has been on the Western excavation area near the rear of the cave and the Eastern and Northeastern excavation areas near the middle of the cave (Fig. 1; Marean et al., 2010). Detailed descriptions of the excavation methods, stratigraphy, and sediment micromorphology at PP13B are presented in Marean et al. (2010) and Karkanas and Goldberg (2010).

Sampling for OSL dating

Thirty-one sediment samples were collected for OSL dating over a number of field seasons since 2001 from all three excavation areas. Thirteen samples were collected from the Western excavation area, eight samples from the Eastern excavation area, and 10 samples from the Northeastern excavation area. Eight of the samples are from non-archaeological units. Figure 1 shows an outline map of the cave on which the position of each OSL sample is indicated in a two-dimensional grid plan of each excavation area. Supplementary Online Material (SOM) Figures 1–9 present the exact location of each sample and its stratigraphic association on a rectified section photograph of the face of the section from which the OSL sample was collected (see SOM published with the online version of this paper).

The connection between the three excavation areas is not yet fully understood due to the variable nature and preservation of the sediments and the changing topography of the basal rocks. Even within an excavated area, preservation of any single-stratigraphic aggregate is complex, with some being truncated off in some but not all quadrants, (e.g., SOM Fig. 4) and others bleeding into each other (e.g., SOM Fig. 3; Marean et al., 2010). As a result, it was not always possible to collect samples for OSL dating from a single, simple stratigraphic column. Where this could be achieved, it was done (e.g., samples 46494–46496 and 46739–46741 in the Eastern excavation area; see SOM Figs. 1 and 3), but in the majority of cases samples were collected from different parts of the excavation. One aim was to collect samples from sedimentary contexts that are most favorable for OSL dating (e.g., sandy, undisturbed sediments). Another aim was to collect samples from as many of the facies as possible to determine whether chronological connections between the different areas exist and to obtain information about the relative continuity, or the lack thereof, for the occupation of the site. This sampling strategy prevents the use of single-grain OSL dating as a general tool for checking the stratigraphic integrity of a site (Jacobs and Roberts, 2007). Instead, it only informs about the age and the integrity of the immediate area from where the samples were collected. Not all samples relate to periods of anthropogenic activity, some represent archaeologically sterile units, but these were collected to inform about the cave life history and the impact that changing environments can have on the availability of a site as a living space.

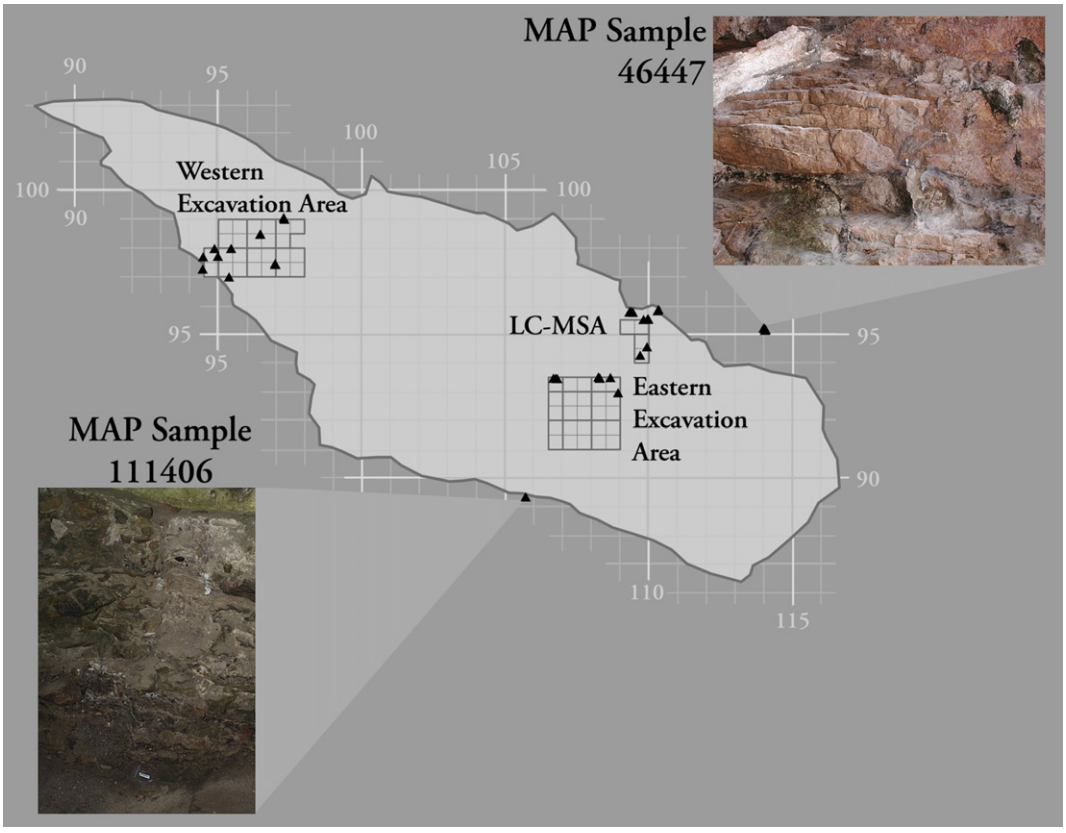

Fig. 1. Map of cave showing location of OSL samples and the excavation areas discussed in the text.

All samples were collected at night with appropriately filtered red torchlight to prevent exposure to sunlight that will zero the OSL signal. Samples were either scraped into a black plastic bag with a teaspoon to prevent inadvertent mixing of grains originating from adjacent units during the sampling process, or where samples were collected from more cemented units (such as the LC-MSA), a small drill bit was used to first loosen the sediment that was then scraped into a light-tight black bag. We have also collected a separate bag of sediment from which the moisture content and dose rate of the samples were determined. We have, therefore, exercised extreme caution to prevent artificial mixing of different stratigraphic layers during the sample collection process.

Tables 1–3 present, for each excavation area, the stratigraphic association of each OSL sample and a synopsis of the sedimentary context of the layers from which samples were collected. These summaries are based on the analyses and descriptions provided in Bernatchez (2010), Marean et al. (2010), and Karkanas and Goldberg (2010), but focus only on those aspects that directly influence the calculation and reliability of the OSL age estimates.

Luminescence dating

Optically stimulated luminescence (OSL) dating provides a means of determining burial ages for sediments. In this study, two different OSL-based methods were employed: conventional OSL dating that uses the 'fast' component in quartz (e.g., Duller, 2004) and thermally transferred OSL (TT-OSL) that involves stimulating an alternative electron trap that is less light sensitive (Adamiec et al.,

Table 1
Stratigraphic, sedimentary context, and sample location information for those samples collected from the Northeastern excavation area[a]

Stratigraphic aggregate	Sample number	General position	Sedimentary context (Bernatchez, 2010; Karkanas and Goldberg, 2010; Marean et al., 2010)
LC-MSA Upper	46447	Upper dune	• Carbonate impregnated aeolian sands
	111400		• Flowstone capping
	46467	Lower dune	• Large root fillings
	20720		• More homogeneous and sandier then LC-MSA Lower
	111401		• *In situ* burnt zones
LC-MSA Middle	111402	Middle	• Some evidence for bioturbation and trampling (LC-MSA Middle)
			• Shell rich layers
LC-MSA Lower	111403	Top	• Layers of greasy organic matter/charcoal rich sediments
	20721	Middle	• Sequence of fine *in situ* fires
	111404	Bottom	• Whitish calcareous lenses
	111406	Middle	• Roof spall, sometimes clast supported (along southern section)
			• Some localized bioturbation
			• Erosional surface

[a] The samples are in stratigraphic order from top to bottom.

Table 2
Stratigraphic, sedimentary context, and sample location information for those samples collected from the Eastern excavation area[a]

Stratigraphic aggregate	OSL sample number	Sedimentary context (Bernatchez, 2010; Karkanas and Goldberg, 2010; Marean et al., 2010)
Surface sediments		
Re-Deposited Disturbance		
Truncation Fill		
Shelly Brown Sand-Upper Roof Spall	46494	• Dispersed fragments of roof spall
	46739	• Less roof spall in upper SBS than in lower URS
	46466	• Shellfish abundant in SBS
	46465	• Thin layers of well preserved hearths containing discrete bands of ash, charcoal, and baked sediment
	46740	
	46495	
Lower Roof Spall	46496	• Roof spall rich in the south, more sandy in the north
	46741	• Cemented patches common in southern parts
		• Fragments of aeolianite in the cemented areas
Bedrock		

[a] The samples are in stratigraphic order from top to bottom.

2008; Pagonis et al., 2008). The conventional OSL dating technique is limited to samples that are less than ~200 ka old at PP13B. Beyond this, quartz grains cannot absorb any more radiation energy since their 'fast component' electron traps have been completely filled (saturated). Few samples studied from PP13B were saturated ($n = 4$), and therefore beyond the dating range of conventional OSL procedures. It was for three of these samples that the TT-OSL method was used instead. Good agreement between the two methods has previously been demonstrated for Chinese loess sediments back to ~125 ka, for which complete zeroing of the TT-OSL signal could be assured, and ages as far back as the Brunhes-Matuyama boundary (~780 ka) were accurately obtained when compared to independently derived ages (Wang et al., 2006, 2007). Details about the technique can be found in Wang et al. (2007) and Tsukamoto et al. (2008). Estimation of the burial age using either conventional OSL or TT-OSL dating follows the same basic principles.

The time elapsed since sediments were last exposed to sufficient heat or sunlight to reset the luminescence 'clock' can be estimated from measurements of the OSL or the TT-OSL, and of the radioactivity of the sample and surrounding materials (Aitken, 1998; Bøtter-Jensen et al., 2003). By measuring the OSL or TT-OSL signal from a sample of sediment, the equivalent dose (D_e) can be determined. This involves comparing the OSL or TT-OSL signal from a 'natural' sample to signals induced in the laboratory after administering known doses using a calibrated radiation source to portions (aliquots or individual grains) of the same sample. The latter signals are used to construct an OSL (Fig. 2a and b) or TT-OSL (Fig. 2c) dose response curve, from which an estimate of the D_e can be made. This is defined as the amount of radiation needed to generate an OSL or TT-OSL signal in the laboratory that is equal to that produced by the natural sample from the dose absorbed since the most recent zeroing event.

Table 3
Stratigraphic, sedimentary context, and sample location information for those samples collected from the Western excavation area[a]

Stratigraphic aggregate	OSL sample number	General position	Sedimentary context (Bernatchez, 2010; Karkanas and Goldberg, 2010; Marean et al., 2010)
Surface sediments			
Northeast Fill	46455	Lower	• Slumped feature
			• Sediment infill
LB Sand 1	46460	Middle above DBS3	• Coarse grained
	46462	Lower above DBS3	• Abundant roof spall
			• Some localized disturbances
DB Sand 2			
LB Sand 2			
DB Sand 3			
LBG Sand	46459	Top	• Aeolian sands derived from beach zone
	46464	Top	• Presence of apatite, bone organic matter
	46463	Middle	• Presence of gypsum and its replacement by anhydrite
	46457	Middle	• Presence of calcareous elements with signs of dissolution
DB Sand 4a			
LBG Sand 2			
DB Sand 4b	46458	Middle	• Burnt charcoal and bone
			• Some localized disturbances
LBG Sand 3			
LBG Sand 4			
LB Silt	46461	Top near LBG Sand	• Poorly sorted silty sand
	46456		• Enriched in roof spall
			• Presence of apatite from guano
			• Evidence for stabilizing surface near the top
Laminated Facies	20724	Top	• Multiple layers of sand and silt
	20730	Middle	• Rounded to subangular grains of quartz
	20735	Bottom	• Breakdown products of roof spall
			• Low-energy water lain deposits
Boulder facies			
Boulder beach			

[a] The samples are in stratigraphic order from top to bottom.

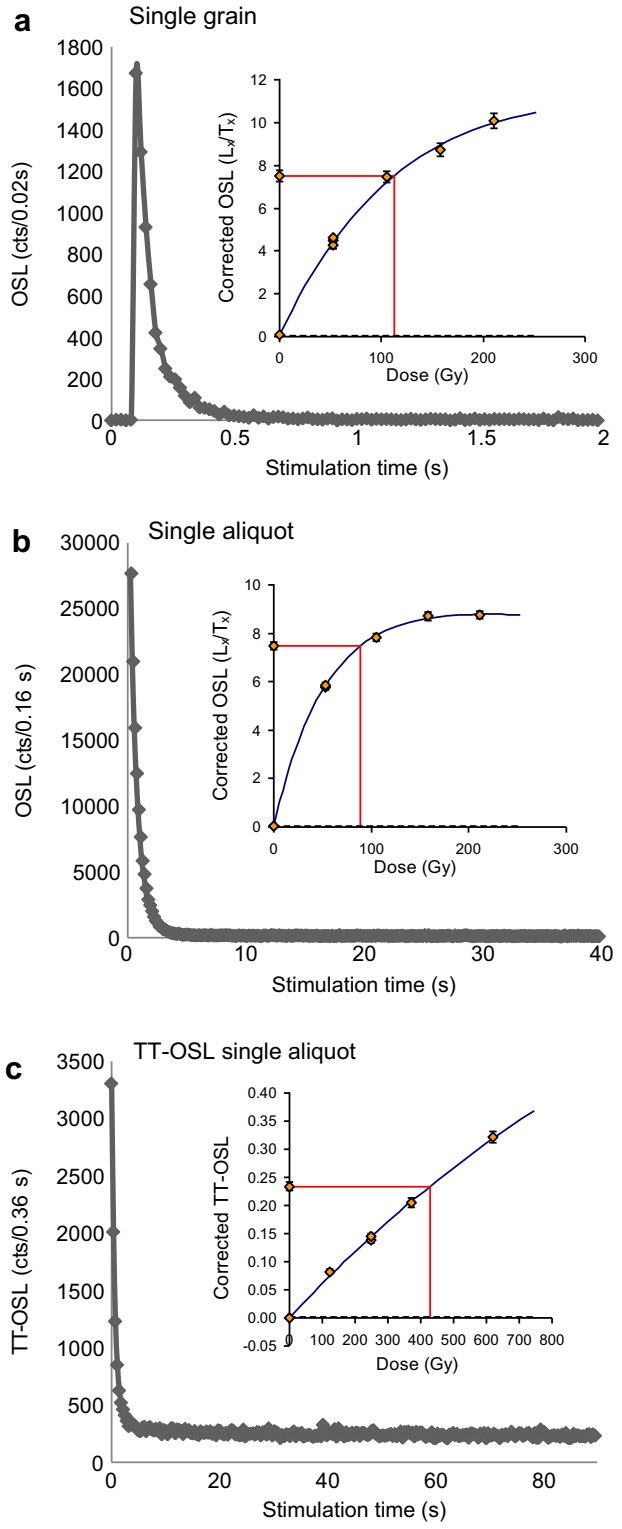

Fig. 2. Decay curves and dose response curves for representative (a) single-grain OSL, (b) single-aliquot OSL, and (c) single-aliquot TT-OSL.

Also estimated is the dose rate (D_r), which represents the rate of supply of ionizing radiation to the sample in its natural environment over the entire burial period. This involves assessing the radioactivity of the sample and the surrounding material, to a distance of about 40 cm, using chemical or physical methods. A burial age estimate of well-bleached or -zeroed grains can then be obtained by dividing the equivalent dose (D_e) by the environmental dose rate (D_r).

Sample preparation

All samples were opened in the laboratory under the appropriate lighting conditions (dim red/orange illumination). Sediments collected for moisture content and dose rate measurements were weighed and dried to obtain estimates of current field moisture contents, and these same sediments were then ground to a fine powder for laboratory determinations of dose rates. All OSL samples were subjected to a series of chemical treatments to isolate quartz grains of a specific size range for the measurement of the OSL signal. Carbonates were dissolved in 10% HCl acid and organic matter was oxidized in 30 vol H_2O_2. The 180–212 μm diameter grain size fraction was then separated by mechanical dry sieving, and the quartz grains were isolated by density separation using sodium polytungstate (SPT) solutions of specific gravity 2.62 (to reduce the potassium rich feldspar content) and 2.70 (to remove heavy minerals). The quartz grains were etched in 48% HF acid for 40 min to destroy any remaining feldspars, and then washed with concentrated HCl acid for 40 min to remove any precipitated fluorides. The etched quartz grains were sieved again, using the smaller mesh diameter (180 μm), and only the grains retained on this sieve were used for dating. This same procedure was systematically applied to each sample. Sufficient material for dating was obtained from all samples.

Equivalent dose (D_e) measurements

Single grains or single aliquots?

A number of studies have recently shown that it is desirable to measure individual grains of quartz to determine the D_e value for a sample, rather than the more conventional single-aliquot approach, where each aliquot consists of several 10 s–1000 s of grains (e.g., Murray and Roberts, 1997; Jacobs et al., 2003b, 2006a,c, 2008b; Olley et al., 2004, Feathers et al., 2006; Porat et al. 2006; Jacobs and Roberts, 2007; Duller, 2008; Tribolo et al., 2010). Measurement of individual grains is particularly beneficial in archaeological contexts where: 1) post-depositional disturbances (Jacobs et al., 2006c, 2008a; David et al., 2007), 2) the effects of beta microdosimetry (e.g., Jacobs et al., 2008b, c), and 3) the possibility of roof spall contamination and other forms of non-homogeneous bleaching (Roberts et al., 1998, 1999) are of concern. These can produce 'contaminant' grains that can skew the age estimate of a sample if not identified and removed prior to age calculation. The archaeological sediments at PP13B show potential for all three of the major concerns discussed above (see Tables 1 to 3); roof spall appears in abundance in some units, localized disturbances have been documented, and the presence of bioclastic fragments, apatite, gypsum, and carbonates may affect the beta dose rate estimated in the laboratory (see Bernatchez, 2010; Karkanas and Goldberg, 2010; Marean et al., 2010). The potential effect of any of these factors on the estimation of an OSL age is variable across the site and each sample should, therefore, be assessed on an individual basis. As a result, we have measured the 23 samples collected from archaeological units exclusively with single grains in order to identify any 'contaminant' grains, determine their likely origin or cause, and exclude them from the data set before final age determination (Jacobs and Roberts, 2007).

There are, however, situations where single-grain dating is not necessary or not possible. Where stratigraphic integrity can be assured and sediment mixing discounted, multigrain aliquots may be sufficient. At PP13B the four samples collected from

archaeologically sterile, homogeneous, and cemented dune sands observed in the Northeastern excavation area fall in this category. Single aliquots were also measured for the three samples collected from the Laminated Facies, for which the TT-OSL method was used.

Equipment

A Risø TL/OSL-DA-15 optical stimulation and detection system, equipped with a focused laser attachment for optical stimulation of single, sand-sized grains, was used to measure all individual grains in this study. OSL measurements were made using the beam from a 10 mW Nd:YVO_4 diode-pumped green laser (532 nm) focused down to a 10 μm diameter spot with a power density of ~50 W/cm^2 (Bøtter-Jensen et al., 2000). The same Risø system was also used for measurement of the conventional OSL single-aliquot measurements, but a different Risø TL/OSL-DA-20 optical stimulation and detection system was used for the TT-OSL measurements. Both systems are equipped with blue (470 nm) light emitting diodes (LEDs), which were used to measure all single aliquots (OSL and TT-OSL). The ultraviolet OSL emissions from single grains and single aliquots were detected using Electron Tubes Ltd 9635Q photomultiplier tubes fitted with 6 mm of Hoya U-340 filter. Laboratory irradiations were given to all single grains and single aliquots using calibrated $^{90}Sr/^{90}Y$ beta sources mounted on the Risø instruments.

Single grains were mounted on discs that had a 10 × 10 grid of 300 μm diameter holes drilled in the surface, each hole being able to contain one grain of ~200 μm in diameter; in total 21,100 grains were measured in this way. For the single-aliquot OSL measurements, aliquots were prepared by spreading grains on a disc that had been sprayed with silicone oil, through a mask with holes 0.5 mm in diameter; this diameter circle enabled about 10 grains per aliquot (Duller, 2008). Forty-eight aliquots were measured for each sample. For the single-aliquot TT-OSL measurements, aliquots 5 mm in diameter were prepared, enabling ~100 grains per aliquot. Only 10 aliquots were measured for each sample since these measurements are significantly more time consuming than conventional OSL measurements. The large size of the aliquots was necessary to obtain adequate counting statistics and noise free decay curves from the TT-OSL signal (e.g., Wang et al., 2007).

Equivalent dose (D_e) determination of individual aliquots and grains

To determine the D_e value for both single grains and single aliquots of quartz, the single aliquot regenerative dose (SAR) procedure (Galbraith et al., 1999; Roberts et al., 1999; Murray and Wintle, 2000) was followed. The approach followed in this study mimics that presented for the aeolian sands from Blombos Cave (single aliquots; Jacobs et al., 2003a) and the archaeological sediments from a range of MSA sites in Southern Africa (single grains; Jacobs et al., 2008c). The procedures involved a preheat temperature of 240 °C for 10 s prior to measurement of the OSL resulting from the natural (L_N) and regenerative (L_x) doses, and a preheat of 160 °C for 5 s prior to measurement of the OSL from the test doses (T_N and T_x). The main OSL measurements (L_N and L_x) and the responses to the test doses (T_N and T_x) were made at a temperature of 125 °C, with stimulation of single aliquots and single grains being for 40 s and 2 s, respectively. The OSL signal from single aliquots was determined from the first 0.48 s of data, using the final 8 s to estimate the background count rate. For single grains, the first 0.22 s of data was used for determination of the OSL signal and the last 0.33 s for background count rates. An example single grain and single aliquot decay curve are presented in Figure 2a and b.

The single-aliquot TT-OSL measurement approach is more involved and the basic method is described in detail in Wang et al. (2006, 2007). Description and discussion of the technique is beyond the scope of this paper since only three of the samples were measured in this way. We followed the general measurement procedure of Tsukamoto et al. (2008). This involves a preheat of 280 °C for 10 s prior to the depletion of the fast and medium components at 125 °C for 300 s. A preheat of 280 °C for 10 s was then used for the natural and regenerative doses prior to measurement of both the thermally transferred OSL ($L_{TT\text{-}OSL}$) and basic transferred OSL ($L_{BT\text{-}OSL}$) signals and a preheat of 220 °C for 5 s was applied prior to all test dose measurements. The $L_{TT\text{-}OSL}$ and $L_{BT\text{-}OSL}$ measurements (L_x) and the responses to the test doses (T_x) were made at a temperature of 125 °C with stimulation being for 100 s duration. An additional high temperature hot optical wash of 300 °C for 300 s was applied at the end of every measurement cycle to reduce the build up of the unbleachable components of the signal (Jacobs et al., 2006b). This temperature was experimentally determined to be the most appropriate for the samples from Pinnacle Point. The $L_{TT\text{-}OSL}$, $L_{BT\text{-}OSL}$, and T_x signals were determined from the first 1.2 s of data, using the final 20 s to estimate the background count rate. An example TT-OSL decay curve is shown in Figure 2c.

Full dose response curves were constructed for OSL and TT-OSL single aliquots and single grains using at least six regenerative dose points for all aliquots. The size of the regenerative doses ranged between 20 Gy and 210 Gy for single aliquot and single grain OSL measurements and between 100 Gy and 600 Gy for TT-OSL measurements. Both types of measurements also included a 0 Gy dose and a repeat dose point as a test of reproducibility ('recycling'). The test dose was ~2 Gy for OSL and TT-OSL single aliquots and ~9 Gy for single grains. The regenerative dose points for all aliquots and grains were fitted with a saturating exponential plus linear curve (Fig. 2a–c).

Routine checks of OSL and TT-OSL protocol performance were made for thermal transfer, test dose sensitivity correction, and dose response behavior (Jacobs et al., 2003b, 2006a). Multigrain aliquots and single grains were rejected if they had thermally transferred signals >5% of the natural OSL at zero-applied dose, 'recycling ratios' (i.e., the reproducibility of a replicate dose point) that were more than two standard deviations different from unity, and dose response curves that were saturated or did not intercept the natural OSL signal. Single grains were also rejected if their test dose OSL signals (measured after stimulation of the natural OSL) were statistically indistinguishable from background.

To test the appropriateness of the OSL experimental and analytical procedures, grains of one sample from each excavation area were bleached in natural sunlight for several days before any measurement and given a known dose similar to the expected D_e value (i.e., a dose recovery test). The correct dose estimates were obtained from multigrain aliquots; these samples gave ratios of measured/given dose of 0.97 ± 0.04 (111403; Northeastern area), 0.96 ± 0.03 (46465; Eastern area), and 1.03 ± 0.04 (46463; Western area). A single-grain OSL dose recovery test was also conducted for sample 46463 from the Western area using the same procedures as above. The given dose was 120 Gy and the weighted mean measured dose was 116 ± 4 Gy with an overdispersion value of 13 ± 3%. The given and measured dose values are statistically consistent within 1σ and the overdispersion is typical for single-grain dose recoveries (e.g., Galbraith et al., 2005; Jacobs et al., 2006a). A TT-OSL dose recovery test was also performed on modern beach sand that was collected from the front of the PP13 cave complex. It was given a 400 Gy dose and the weighted mean measured dose from 10 aliquots was 412 ± 15 Gy. These dose recovery test results confirm that the measurement conditions used are appropriate for the samples from PP13B.

Uncertainties on the D_e

The reported measurement error associated with the D_e value (determined using both OSL and TT-OSL measurement procedures)

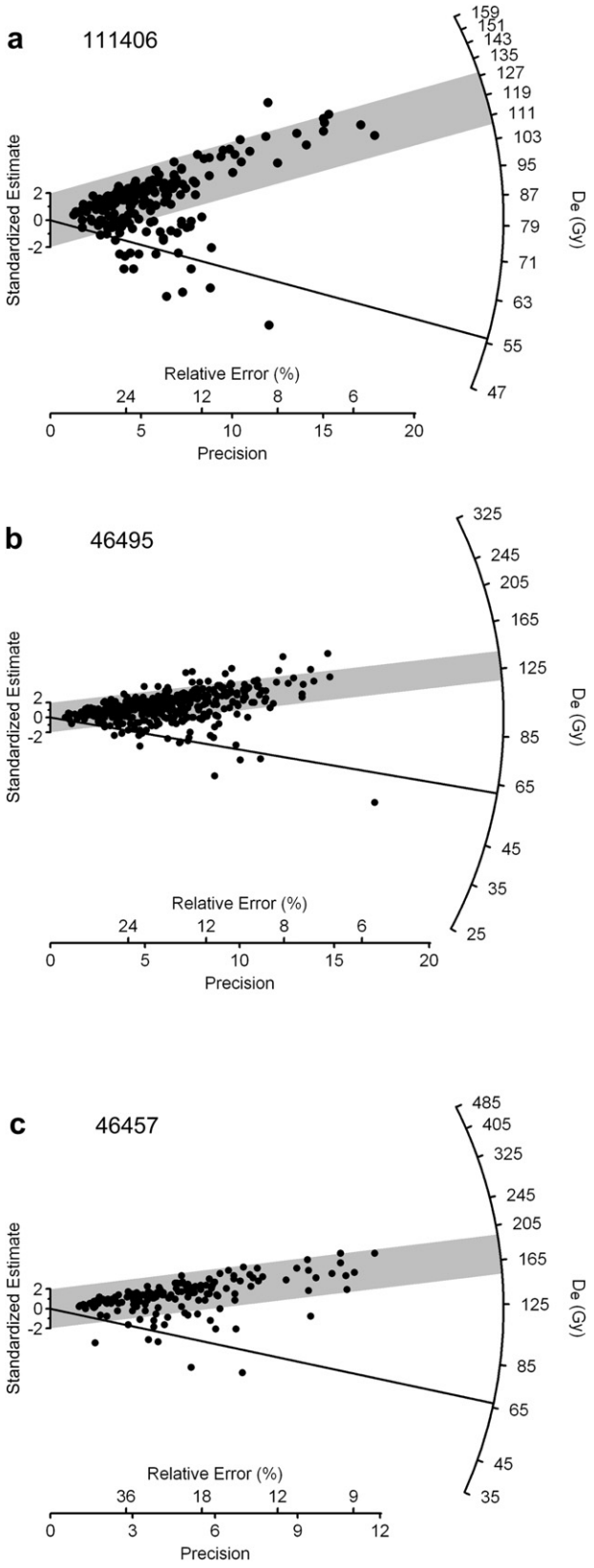

Fig. 3. Radial plots of single-grain D_e values for a representative sample from each of the three excavation areas: (a) Northeastern excavation area (111406), (b) Eastern excavation area (46495), and (c) Western excavation area (46457). The reference value for the gray shading is the 'central' D_e and its 95% confidence interval, calculated using the finite mixture model for the component with the greatest proportion of grains. The gray line shows the central D_e value for the minor D_e component obtained using the finite mixture model.

for each aliquot and grain consists of the quadratic sum of a number of different 'random errors.' Some of these 'random errors' can be reduced in size by making many repeat measurements and combining the individual D_e values using an appropriate statistical model (e.g., Galbraith et al., 1999). In this study, the 'random error' is based on counting statistics associated with each OSL measurement (L_x and T_x) and curve fitting uncertainties related to the construction of each dose response curve, obtained from the standard error on the D_e determined by Monte Carlo simulation (Yoshida et al., 2003; Duller, 2007). In addition, allowance is also made for uncertainties associated with instrument reproducibility which is added in quadrature to every measurement of L_x and T_x: 1% error for each single-aliquot OSL and TT-OSL measurement and 2% error for each single-grain OSL measurement (Jacobs et al., 2006a). The reported standard error at 1σ for the final D_e, which corresponds to the 68% confidence limits (i.e., there is a one in three chance that the true age will lie outside the ±1σ) in the case of a Gaussian distribution, also includes a 'systematic error.' This error always remains constant and cannot be reduced by making more measurements and, therefore, ultimately dominates the precision of our final D_e value. In this study, a 'systematic error' of 2% was added quadratically to the final D_e estimate to account for the uncertainty associated with calibration of the laboratory beta source.

Analysis and interpretation of D_e distributions

To identify any 'contaminant' grains and to estimate the true burial dose from a distribution of D_e values, their distribution patterns were visually examined (Jacobs and Roberts, 2007). The radial plot (e.g., Fig. 3a–c) was used for graphical display since it simultaneously provides information about the spread, precision, and statistical consistency of the D_e values (Galbraith, 1988, 1990). The shape of the radial plot can take on certain types of patterns that can reveal which one or combination of the factors discussed above is responsible for the presence of 'contaminant' grains and, therefore, spread in the D_e distribution (Jacobs and Roberts, 2007). The amount of spread was also quantified by the value of overdispersion that takes into account the scatter due to measurement error; if all of the scatter were the result of measurement error the overdispersion value would be zero (Galbraith et al., 1999). It is, however, common in OSL studies of archaeological and geomorphological sediments to observe some overdispersion for samples that are known to have been well bleached prior to deposition due to natural and physical variability (e.g., Olley et al., 2004; Jacobs et al., 2006a). Once the radial plot and overdispersion of a sample have been assessed, and the D_e distribution interpreted in association with an understanding of the sedimentary and archaeological context of the sample, there are several statistical models available that can be used to combine the individual D_e values meaningfully to obtain the best estimate of D_e from an overdispersed single-grain D_e distribution.

In this study we employed two different types of statistical models. Where D_e distributions were interpreted to represent a single well-bleached population of grains (i.e., the radial plot shows no discrete patterns and the overdispersion value is relatively small), the central age model (CAM) was applied. This model assumes that the D_e values for all grains are centered on some average value of D_e (similar to the median) and the estimated standard error takes account of any overdispersion (Galbraith et al., 1999). When post-depositional mixing, or scatter due to the effects of beta microdosimetry, has been identified as the most likely reason for the presence of multiple, discrete components in a D_e distribution, the number of components, the D_e value of each component, their corresponding uncertainties, and the proportion of grains in each component were estimated using the finite mixture model (FMM; Roberts et al., 2000; Galbraith, 2005). This

Table 4
Dose rate data, D_e values, and optical ages for 31 sediment samples from PP13B

Sample code	Moisture content (%)	Radionuclide concentrations [a]			Dose rates (Gy ka^{-1})			Total dose rate [b, c] (Gy ka^{-1})	D_e [b, d] (Gy)		Number of aliquots or grains [e]	Overdispersion [f] (%)	Optical age [b] (ka)
		U (μg g^{-1})	Th (μg g^{-1})	K (%)	Beta	Gamma	Cosmic						
Western excavation													
46455	10 ± 2	2.73 ± 0.22	4.29 ± 0.70	0.50 ± 0.05	0.71 ± 0.04	0.57 ± 0.04	0.010	1.33 ± 0.06	3 ± 0.4	(M)	23/24	85 ± 13	2.3 ± 0.3
46460	12 ± 2	2.35 ± 0.25	5.94 ± 0.80	0.47 ± 0.06	0.65 ± 0.04	0.57 ± 0.05	0.010	1.26 ± 0.06	113 ± 2	(S)	142/1000	18 ± 2	90 ± 5
46462	12 ± 2	3.65 ± 0.20	3.04 ± 0.63	0.39 ± 0.05	0.75 ± 0.04	0.57 ± 0.04	0.010	1.36 ± 0.05	123 ± 4	(S)	90/1000	19 ± 2	90 ± 5
											Weighted average		90 ± 4
46459	12 ± 2	3.18 ± 0.26	4.65 ± 0.82	0.43 ± 0.06	0.72 ± 0.05	0.60 ± 0.05	0.010	1.37 ± 0.07	134 ± 3	(S)	158/1000	19 ± 2	98 ± 6
46464	12 ± 2	4.34 ± 0.29	3.50 ± 0.90	0.28 ± 0.07	0.76 ± 0.04	0.64 ± 0.05	0.010	1.44 ± 0.07	143 ± 3	(S)	118/1000	14 ± 2	99 ± 5
											Weighted average		99 ± 4
46463	12 ± 2	1.89 ± 0.24	4.39 ± 0.76	0.39 ± 0.06	0.54 ± 0.03	0.46 ± 0.04	0.010	1.04 ± 0.06	131 ± 4	(S)	118/1000	16 ± 3	127 ± 8
46457	12 ± 2	3.04 ± 0.22	4.14 ± 0.70	0.49 ± 0.05	0.72 ± 0.04	0.58 ± 0.04	0.010	1.34 ± 0.06	164 ± 3	(S)	162/900	13 ± 2	122 ± 6
											Weighted average		124 ± 5
46458	12 ± 2	2.38 ± 0.22	4.39 ± 0.69	0.47 ± 0.05	0.67 ± 0.05	0.52 ± 0.04	0.010	1.24 ± 0.07	197 ± 4	(S)	165/1000	27 ± 3	159 ± 8
46461	18 ± 4	3.27 ± 0.25	3.27 ± 0.79	0.32 ± 0.06	0.59 ± 0.05	0.50 ± 0.04	0.010	1.13 ± 0.06	177 ± 5	(S)	188/1000	25 ± 2	157 ± 10
46456	10 ± 2	3.07 ± 0.28	5.43 ± 0.90	0.47 ± 0.07	0.72 ± 0.04	0.62 ± 0.05	0.010	1.37 ± 0.06	Saturated				
20724[g]	10 ± 2	2.07 ± 0.19	4.13 ± 0.61	0.07 ± 0.01	0.37 ± 0.03	0.43 ± 0.03	0.010	0.85 ± 0.04	326 ± 11	(M)	10/10	5 ± 4	384 ± 23
20730[g]	10 ± 2	2.18 ± 0.16	3.34 ± 0.51	0.32 ± 0.02	0.52 ± 0.03	0.43 ± 0.03	0.010	1.00 ± 0.04	387 ± 10	(M)	10/10	2 ± 5	387 ± 20
20735[g]	10 ± 2	2.15 ± 0.18	4.38 ± 0.59	0.36 ± 0.02	0.56 ± 0.03	0.43 ± 0.03	0.010	1.04 ± 0.04	395 ± 27	(M)	10/10	17 ± 6	380 ± 31
											Weighted average		385 ± 17
Eastern excavation													
46494	12 ± 2	1.54 ± 0.18	3.37 ± 0.59	0.58 ± 0.05	0.63 ± 0.03	0.42 ± 0.03	0.016	1.10 ± 0.05	108 ± 2	(S)	195/1000	19 ± 2	98 ± 5
46739	12 ± 2				0.65 ± 0.04	0.42 ± 0.02	0.016	1.12 ± 0.04	105 ± 4	(S)	130/1000	23 ± 3	94 ± 5
46466	12 ± 2	2.22 ± 0.24	5.52 ± 0.77	0.53 ± 0.06	0.74 ± 0.04	0.57 ± 0.04	0.016	1.36 ± 0.06	125 ± 3	(S)	169/900	21 ± 2	92 ± 5
46465	12 ± 2	2.07 ± 0.24	5.54 ± 0.76	0.58 ± 0.06	0.73 ± 0.04	0.56 ± 0.04	0.016	1.34 ± 0.06	122 ± 4	(S)	85/500	17 ± 3	91 ± 5
46740	12 ± 2				0.69 ± 0.04	0.42 ± 0.02	0.016	1.15 ± 0.04	111 ± 5	(S)	263/1000	21 ± 2	96 ± 6
											Weighted average		94 ± 3
46495	12 ± 2	1.28 ± 0.24	3.31 ± 0.44	0.65 ± 0.04	0.62 ± 0.03	0.41 ± 0.03	0.016	1.08 ± 0.04	122 ± 2	(S)	440/1000	21 ± 1	113 ± 5
46496	12 ± 2	1.60 ± 0.13	2.85 ± 0.40	0.64 ± 0.04	0.65 ± 0.03	0.41 ± 0.02	0.016	1.11 ± 0.04	122 ± 2	(S)	176/1000	18 ± 2	110 ± 5
46741	12 ± 2				0.62 ± 0.04	0.42 ± 0.02	0.016	1.08 ± 0.04	119 ± 3	(S)	177/800	12 ± 3	110 ± 5
											Weighted average		
Northeastern excavation													
LC-MSA Upper (Upper dune)													
46447	5 ± 1	1.96 ± 0.11	1.54 ± 0.34	0.21 ± 0.03	0.40 ± 0.02	0.33 ± 0.02	0.037	0.80 ± 0.03	74 ± 2	(M)	36/48	13 ± 2	93 ± 5
111400	5 ± 1	1.92 ± 0.11	1.53 ± 0.33	0.18 ± 0.03	0.38 ± 0.03	0.32 ± 0.02	0.037	0.77 ± 0.04	71 ± 2	(M)	42/48	13 ± 2	93 ± 6
											Weighted average		93 ± 4
LC-MSA Upper (Lower dune)													
46467	5 ± 1	1.64 ± 0.09	1.36 ± 0.28	0.31 ± 0.03	0.43 ± 0.02	0.31 ± 0.02	0.016	0.78 ± 0.03	98 ± 3	(M)	40/48	10 ± 2	125 ± 6
20720	5 ± 1	0.84 ± 0.07	1.45 ± 0.21	0.62 ± 0.04	0.37 ± 0.02	0.30 ± 0.02	0.016	0.71 ± 0.03	91 ± 2	(M)	43/48	7 ± 1	128 ± 5
111401	5 ± 1	2.66 ± 0.14	1.36 ± 0.41	0.29 ± 0.04	0.49 ± 0.03	0.29 ± 0.03	0.016	0.83 ± 0.04	101 ± 3	(S)	58/1000	6 ± 4	122 ± 8
											Weighted average		126 ± 5
LC-MSA Middle													
111402	15 ± 3	1.98 ± 0.17	3.03 ± 0.52	0.46 ± 0.04	0.60 ± 0.03	0.29 ± 0.03	0.016	0.93 ± 0.05	117 ± 2	(S)	381/1000	25 ± 1	125 ± 7
LC-MSA Lower													
111403	15 ± 3	1.27 ± 0.11	1.82 ± 0.33	0.34 ± 0.03	0.40 ± 0.02	0.27 ± 0.02	0.016	0.71 ± 0.03	114 ± 2	(S)	164/1000	18 ± 2	160 ± 8
111404	15 ± 3	2.85 ± 0.21	3.22 ± 0.66	0.32 ± 0.05	0.57 ± 0.03	0.47 ± 0.04	0.016	1.09 ± 0.05	116 ± 3	(S)	168/1000	28 ± 2	106 ± 6
20721	15 ± 3	1.56 ± 0.14	2.98 ± 0.45	0.17 ± 0.01	0.36 ± 0.03	0.31 ± 0.02	0.016	0.72 ± 0.05	119 ± 3	(S)	127/1000	14 ± 2	166 ± 9

Table 4 (*continued*)

Sample code	Moisture content (%)	Radionuclide concentrations [a]			Dose rates (Gy ka^{-1})			Total dose rate [b, c] (Gy ka^{-1})	D_e [b, d] (Gy)		Number of aliquots or grains [e]	Overdispersion [f] (%)	Optical age [b] (ka)
		U (μg g^{-1})	Th (μg g^{-1})	K (%)	Beta	Gamma	Cosmic						
LC-MSA Lower (South wall)													
111406	15 ± 3	1.00 ± 0.15	2.99 ± 0.47	0.38 ± 0.04	0.40 ± 0.02	0.30 ± 0.03	0.016	0.74 ± 0.04	119 ± 4	(S)	194/1000 Weighted average	29 ± 2	162 ± 8 162 ± 6[h]

[a] Measurements made on subsamples of dried, homogenized, and powdered sample by thick source alpha counting (TSAC; for U and Th) and a combination of TSAC and GM-25-5 beta-counting to obtain an estimate of ^{40}K. Dry dose rates calculated from these activities were adjusted for the water content (expressed as % of dry mass of sample).
[b] Mean ± total uncertainty (68% confidence interval), calculated as the quadratic sum of the random and systematic uncertainties.
[c] Includes an assumed internal alpha dose rate of 0.03 Gy ka^{-1} with an assigned relative uncertainty of ±25%.
[d] Estimated using multigrain aliquots (M) or single grains (S). Single grain D_e values were obtained using either the finite mixture model to determine the D_e for the dose component represented by the highest proportion of grains or the central age model. The total uncertainty includes a systematic component of ±2% associated with laboratory beta source calibration.
[e] Number of multigrain aliquots or individual grains used for D_e determination/total number of aliquots or grains analyzed.
[f] Relative standard deviation of the D_e distribution after allowing for measurement uncertainties.
[g] Samples for which the D_e value was obtained using the TT-OSL method.
[h] Sample 111404 was not included in the calculation of the weighted average.

model is more complicated than the CAM but has been shown to successfully identify known D_e components from composite data sets (e.g., Roberts et al., 2000; Jacobs, 2005; Jacobs et al., 2006c). Worked examples and detailed descriptions of the application of the FMM to archaeological deposits are provided in David et al. (2007) and Jacobs et al. (2008a). Those procedures are identical to the procedures employed in this study.

The D_e distributions for all the samples are presented as radial plots and discussed below for the three different excavation areas. Information about the number of grains measured and used, the overdispersion values calculated, statistical models used, and the final $D_e \pm 1\sigma$ value for each sample is presented in Table 4.

Northeastern excavation area

A series of multiple grain aliquot and single-grain measurements were made for 10 samples collected from the Northeastern excavation area. Results for these samples were presented in Marean et al. (2007). The results for multigrain single aliquots for the samples collected from the archaeological sediments showed overdispersion values (15–23%) that were larger than those observed for the sterile dune sands (6–13%) overlying them. The possibility of post-depositional mixing of grains or other factors that may influence the OSL measurements could not be discounted. Accordingly, individual grains of these samples were measured, and based on the results the multigrain data are now discarded. The samples from the upper and lower dune sands are now 1.05 times larger, whereas those from the LC-MSA Lower are 0.99 times smaller than the values published by Marean et al. (2007).

The D_e distributions for the samples from the three different stratigraphic aggregates (LC-MSA Lower, Middle, and Upper) are discussed separately because of differences in their appearance and interpretation.

LC-MSA Lower

A total of 4,000 grains were measured for the four samples collected from the LC-MSA Lower. Not every grain that is measured results in usable OSL data and grains were rejected using the criteria described and tested elsewhere (Jacobs et al., 2003b, 2006a). For samples from the LC-MSA Lower, between 13% (20721) and 19% (111406) of the grains were usable for calculation of individual D_e values. The D_e values for the grains that were not rejected are displayed as radial plots for all the samples in SOM Figure 10g–j. A radial plot for a representative sample from the LC-MSA Lower level (111406) is also presented in Figure 3a.

The calculated overdispersion values for these samples (Table 4) range between 14 ± 2% (27021) and 29 ± 2% (111406). In Marean et al. (2007), these D_e distributions were interpreted as providing evidence for small-scale sediment mixing and the FMM was applied. Application of the FMM resulted in the recognition of two discrete D_e components in each of the samples. To calculate the final D_e value for these samples (Table 4), the weighted mean D_e and standard error for the D_e component containing the greatest proportion of single grains were used (SOM Fig. 10g–j).

Since publication of these ages, further investigations revealed that the 'minor' D_e component (represented by the smallest proportion of grains) for the samples from the LC-MSA ranged between 11 ± 3% (sample 111403) and 30 ± 5% (sample 111404) is unlikely to be the result of post-depositional mixing or downward intrusion of grains from younger overlying units. There are two reasons for this change in interpretation: 1) the D_e values obtained for these 'minor' D_e components range between 55 ± 4 Gy (111406) and 81 ± 4 Gy (20721) and are smaller than the D_e values of any of the immediately overlying samples, and 2) analysis of the dip and

strike of the finds in these layers shows little or no dramatic or random changes that would indicate intrusions or disturbances (Bernatchez, 2010). This is supported by sediment micromorphology (Karkanas and Goldberg, 2010). Instead, it is likely that these 'minor' D_e components are the result of spatially inhomogeneous sources of radioactivity at the scale of a few millimeters, delivering variable beta doses to individual grains (i.e., 'beta microdosimetry'). This occurrence is not unusual and has been demonstrated for the sediments at both Sibudu (Jacobs et al., 2008b) and Diepkloof (Jacobs et al., 2008c). At PP13B the LC-MSA Lower sediments contain multiple lenses of carbonaceous material that appear to be heavily burnt and represent both *in situ* combustion features and evidence for spread of burnt material through trampling. The carbonaceous material is often inert with regards to its radioactivity and provides a lower beta dose rate to the grains, resulting in lower D_e values for grains that abut or that are surrounded by more than 2 mm of such materials. The rationale, methods of detection, and correction is described in detail in Jacobs et al. (2008b) and is identical to the method employed at PP13B. The procedure for the calculation of the final D_e, using the FMM is the same as when mixing occurs and, therefore, did not change the D_e values reported in Marean et al. (2007). It will, however, influence the final age estimates as it requires a correction to be made to the beta dose rate and this will be discussed in the section on dose rates below. The final $D_e \pm 1\sigma$ values for these samples are presented in Table 4.

LC-MSA Middle

One thousand grains were measured for a single sample (111402; SOM Fig. 10f) from LC-MSA Middle, and D_e values could be calculated for ~ 38% ($n = 381$) of the grains. This is a much greater proportion of the measured grains compared to the ~16% of the LC-MSA Lower and ~6% of the LC-MSA Upper. This increase in the 'OSL sensitivity' (brightness) of the grains likely reflects the degree of burning that has taken place in this phase. When a quartz grain is exposed to high temperatures a change in sensitivity takes place, resulting in an increased intensity of the measured signal per unit-absorbed dose (Chen et al., 2001). This has previously been observed for sediments at Sibudu (Jacobs et al., 2008a) and Diepkloof (Jacobs et al., 2008c), which have clear macro- and microscopic evidence of intense burning (e.g., Goldberg et al., 2009), and at Blombos Cave where one OSL sample (ZB8) was deliberately collected from a hearth (Jacobs et al., 2006c). The composition of the LC-MSA Middle sediments supports this suggestion for an increased 'sensitivity' of the OSL signal. The sediments comprise multiple lenses of dark organic material that includes charcoal and *in situ* hearths and much of the deposit is ash, which proportionally is more in the Middle than in the Lower LC-MSA (Karkanas and Goldberg, 2010).

As in the case of LC-MSA Lower, we previously interpreted the pattern of the D_e values when displayed on a radial plot (SOM Fig. 10f), together with its overdispersion value of $25 \pm 1\%$, as evidence for sediment mixing. The FMM identified 40% of the D_e values from this sample as being 'intrusive' (that is, grains with D_e values that do not form part of the main D_e component). Unlike the LC-MSA Lower, the slope of the plotted finds from LC-MSA Middle shows the presence of areas of downward disturbance (Bernatchez, 2010), and sediment micromorphology investigations revealed the existence of ancient root casts that penetrated through the LC-MSA Upper into the LC-MSA Middle. These large roots could, therefore, have introduced younger grains into the otherwise older underlying deposits. The range of D_e values observed for the 'minor' D_e component captures the range expected from grains derived from both the upper (~75 Gy) and lower (~95 Gy) dune sand in the LC-MSA Upper. It is, therefore, not possible to dismiss mixing as a likely mechanism. However, we cannot exclude the contribution from beta microdosimetry. These sediments are just as likely, if not more so, to suffer from its effects due to the presence of ash, organics, the calcite that replaced the roots and appear as white pipes, carbonate-cement, and the presence of cobbles and roof spall (Marean et al., 2007, 2010; Karkanas and Goldberg, 2010). To err on the side of caution, a small correction for the possible impact of beta microdosimetry was made to the beta dose rate for this sample, but the final D_e value, as presented in Marean et al. (2007), remains the same.

LC-MSA Upper

Most of the samples from the LC-MSA Upper were measured using multiple grain aliquots consisting of ~10 grains. These samples represent cemented aeolian dune sand overlying the archaeological sediments. On the basis of their geomorphological features and cemented nature, it was assumed that the sediments are undisturbed, as well as homogeneous with regards to bleaching and environmental dose rate. But to check the reliability of our assumption and measurements, we also measured 1,000 single grains for one of these samples (111401). Only 58 D_e values were obtained with an overdispersion value of $5 \pm 2\%$. This low number of usable grains for which D_e values could be calculated is typical for sand dunes along the southern Cape coast (e.g., Jacobs et al., 2003b; Carr et al., 2007). Using the central age model (CAM), a single-aliquot D_e estimate of 95 ± 3 Gy and a single-grain D_e estimate of 101 ± 4 Gy were calculated. These two values are statistically consistent with each other at the 68% confidence limit (ratio of 1.06 ± 0.06). This consistency in the results provides confidence in our age estimates for these units where single aliquots, rather than single grains, were used to determine the D_e value. The assumptions that the upper and lower dune sands within the LC-MSA Upper had been well bleached at burial and represent single-depositional events are also supported by the range of overdispersion values calculated for these samples ($7 \pm 1\%$ to $13 \pm 2\%$) and the appearance of the radial plots (SOM Fig. 10a–e), which show that very few of the single aliquots are not consistent with the weighted average (i.e., only a few D_e values fall outside the 2σ band). The central age model of Galbraith et al. (1999) was used to determine the weighted mean D_e and its standard error for all the samples from the LC-MSA Upper (Table 4).

Eastern excavation area

Only single grains were measured for the samples collected from the Eastern excavation area. A total of 7,400 grains were measured; 5,400 for the six samples from the Shelley Brown Sand-Upper Roof Spall (SBS-URS) facies (SOM Figs. 3 and 4) and 2000 grains for the two samples from the Lower Roof Spall (LRS) facies (SOM Fig. 3). The proportions of grains for which D_e values could be calculated were very similar to those obtained for the LC-MSA Lower and Middle, and ranged between 13 and 44% for the samples from SBS-URS and ~17% for those samples collected from the LRS unit. Again, this increase in OSL sensitivity seen for some of the samples in the SBS-URS facies probably relates to burning for which there is no evidence in the LRS, but ample evidence in the SBS-URS facies in the form of ash, charcoal, and high magnetic susceptibility values from the sediments (Herries and Fisher, 2010; Karkanas and Goldberg, 2010; Marean et al., 2010). The D_e distributions of the samples collected from the Eastern excavation area are much simpler than those observed in the Northeastern area.

The D_e distributions for all samples are presented as radial plots in SOM Figure 11a–h. A radial plot for a representative sample (46495) is also presented in Figure 3b. The D_e distributions for the two samples from the LRS (SOM Fig. 11g and h) have overdispersion values of 18 ± 2 (46496; Fig. 11g) and $12 \pm 4\%$ (46741; SOM Fig. 11h). The D_e distributions for the six samples collected from the SBS-URS

facies (SOM Fig. 11a–f) have overdispersion values ranging between 17 ± 3% (46465; SOM Fig. 11e) and 23 ± 3% (46739; SOM Fig. 11b). Two of the samples (46740 and 46741) show few outliers that do not form any discrete pattern, whereas the rest of the samples have low outlier D_e values (representing between 6% and 15% of the total number of D_e values) that do form a discrete 'minor' D_e component. The FMM was applied to those samples that showed the discrete minor D_e component to aid in determining a possible mechanism for the presence of these grains. Although intrusion of younger grains from the surface at different times in the past cannot be discounted based on the presence of localized disturbances throughout the Eastern excavation area (Bernatchez, 2010), it is more likely that the 'minor' D_e component is due to the effects of beta microdosimetry. In all six samples the ratio of the minor to the main D_e components is about the same (0.5–0.6). This similarity in the proportion and ratios, regardless of their spatial position, proximity to identified disturbances, and evidence, or lack thereof, for burning, suggest that beta microdosimetry, rather than mixing is the mechanism responsible for the wheel spoke appearance of the radial plot. It is unlikely that mixing throughout the deposit in the eastern part of the cave will result in equal mixing proportions. As a result, the central D_e values obtained from the D_e component with the largest proportion of grains are used as representative and an adjustment to the beta dose rate will be made to reflect the possible bias in the beta dose rate received by individual grains of quartz (Jacobs et al., 2008b). The central age model was used for the other two samples (46741 and 46740) as these represent a single well-bleached dose population (SOM Fig. 11h and f, respectively). The sensitivity of the result to the inclusion or exclusion of outliers in these two samples was tested, but their effects were negligible.

Western excavation area

Thirteen samples collected from the Western area were measured. A combination of single-aliquot TT-OSL ($n = 3$) and single-grain OSL ($n = 10$) measurements were made on the samples from this area.

The single-aliquot TT-OSL D_e distributions for the three samples measured for sediments collected from the bottom, middle, and top of the laminated facies are presented as radial plots in SOM Fig. 12a–c. The D_e distributions for all three samples suggest that the grains all form a single well-bleached dose population. It should, however, be kept in mind that the size of the aliquots are relatively large (~100 grains per aliquot) and that the electron trap that is stimulated is more difficult to bleach with sunlight. The sedimentary context of these samples is complex. Sediment micromorphology suggests that the sands are predominantly breakdown products of the roof rock rather than aeolian or marine sands transported in from outside, that it was most likely that these deposits were water lain, and that the sediments were moist during most of the accumulation phase (Karkanas and Goldberg, 2010). The origin of the quartz grains, the dampness of the sediments that will accelerate breakdown of roof spall, and the mode of deposition are problematic for accurate determination of the D_e using the TT-OSL signal, which requires prolonged periods of sunlight exposure to be well bleached (Adamiec et al., 2008). It cannot be assured that these grains were sufficiently bleached prior to deposition and it may result in significant overestimates of the age and should be treated with caution. However, a large degree of bleaching had to have taken place, since the age of the cave rock is much greater than the age obtained for these sediments. Based on their D_e distributions and small degree of overdispersion (2 ± 5% [20730] to 17 ± 6% [20724], the CAM was used to obtain the most representative $D_e \pm 1\sigma$ value for each of the samples.

The sample collected from the base of LB Silt (46456) had OSL signals that were fully saturated when single aliquots and single grains were measured. TT-OSL measurements have not yet been attempted for this sample due to the complexities described above.

The other nine samples were all measured using single-grain OSL dating and a total of 8,900 grains were measured for samples collected from five different stratigraphic aggregates (LB Silt, DB Sand 4b, LBG Sand, LB Sand 1, and Northeast Fill). The proportion of grains for which D_e values could be calculated ranged between 9% and 19% and is similar to, and typical of, unburnt sediment in PP13B. This is unsurprising, since the interfingering sand lenses, rather than the dark archaeologically rich bands, were targeted for OSL dating in the majority of cases.

The D_e distributions for eight of the nine samples, when displayed as radial plots (SOM Fig. 13a–h), have a similar appearance. A radial plot for a representative sample (46457) is presented in Figure 3c. The one sample that appears different is from the Northeast Fill. This sample shows much greater overdispersion (85 ± 13%), which is not surprising as it was collected from a feature indicating recent disturbance. There is no straightforward way to get a representative D_e value from a D_e distribution like this. The best that could be done was to indicate that it is substantially mixed and then to obtain the minimum D_e value and suggest this as the most recent period of deposition or reworking. The minimum age model of Galbraith et al. (1999) was applied to this sample to obtain the final D_e value (Table 4).

The other eight samples all showed two discrete D_e components. As a result, the FMM was applied to the D_e values obtained for all the samples and the statistical tests were used as before. The main D_e components represent between 86% and 97% of the grains, whereas the minor D_e components represent between 3% and 14% of the grains. The presence of the minor D_e components cannot be explained by beta microdosimetry for all the samples. Calculations of the likelihood of it being due to the effects of beta microdosimetry suggest that this is only possible for those samples for which a ratio of >0.45 (similar to the 0.5–0.6 range observed in the Eastern excavation area) was obtained when the weighted D_e value for the minor D_e component was divided by the weighted mean D_e value of the main component (Jacobs et al., 2008b). Such a ratio indicates that the smallest D_e values are consistent with grains receiving no beta dose. These ratios are based on the relative proportion of the beta and gamma dose rates for these samples, so it should not be used as a universally applicable value for samples from other studies. Samples for which the ratios could explain the effects of beta microdosimetry were samples 46462, 46459, 46464, and 46458 and a correction, based on the proportion of grains in each dose component, was made to the measured beta dose rate (see Jacobs et al., 2008b). The D_e values of the minor dose components for the remainder of the samples are all too small and can only be due to the intrusion of younger grains into the older deposits. For these samples, no correction to the beta dose rate was required. The central D_e value of the main components obtained using the FMM was used for final age calculation for all the samples (Table 4).

Environmental dose rate measurements

The total dose rate for all 31 samples was calculated as the sum of the beta and gamma dose rates due to ^{238}U, ^{235}U, ^{232}Th (and their decay products), and ^{40}K. The concentrations of radioactive elements were measured by Thick Source Alpha Counting (TSAC) and Risø GM-25-5 beta-counting (Bøtter-Jensen and Mejdahl, 1988). These values were converted to dose rates (Adamiec and Aitken, 1998), making allowance for beta dose attenuation (Mejdahl, 1979), HF etching (Bell and Zimmerman, 1978), and sample moisture content (Aitken, 1985). The sample moisture contents were based on the current field moisture estimates and a 20% uncertainty was applied to each of the estimates. Moisture contents obtained before any excavation of the LC-MSA Lower and

Middle in the Northeastern excavation area ranged between 12% and 18%. The LC-MSA Upper was much drier with values ranging between 3 and 5%. Estimates for samples collected from sections that have been excavated in previous seasons resulted in much lower estimates (2–6%), probably due to the desiccation of sediments in sections that have now been exposed to the sun and air. Micromorphology suggested that the LC-MSA Lower was for some period of time a super-saturated environment; however, since we are interested in an average over the entire period of sample burial, an estimate of $15 \pm 3\%$ was considered appropriate and this was applied to all samples collected from the LC-MSA Lower and Middle. A moisture-content estimate of $5 \pm 1\%$ was used for the LC-MSA Upper. The measured moisture contents for samples from the Eastern excavation area ranged between 6% and 11% and for samples from the Western excavation area between 10% and 18%. The total dose rates decrease (and the optical ages increase) by ~1% for each 1% increase in water content.

No high-resolution gamma spectrometry measurements were made to test for disequilibrium in the uranium (U) decay chain (e.g., Jacobs et al., 2006c, 2008a). However, any time dependent complications arising from loss or addition of parental uranium are minimized by measuring the lower part of the U-chain, which is achieved using the laboratory methods employed in this study (Olley et al., 1997). The close agreement between the OSL ages and the U-series ages on flowstone support this notion (see Marean et al. [2007, 2010]). Secular equilibrium, under the assumption that the present day dose rates prevailed throughout the period of sample burial, was assumed.

Account was also taken of the cosmic-ray contribution, which was adjusted for site altitude (15 m), geomagnetic latitude (−33°), the density and thickness of rock (2.5 g/cm^3; sandstone), and sediment (2.0 g/cm^3) overburden (Prescott and Hutton, 1994), as well as the $\cos^2 \Phi$-zenith angle dependence (Smith et al., 1997). The latter dependence was modeled for the three different excavation areas but had a negligible impact on the total cosmic-ray dose rate. The effective alpha dose rate from radioactive inclusions internal to the quartz grains (estimated from measurements made previously on quartz grains from the southern Cape coast; Jacobs et al., 2003a) was also included.

The uncertainty attached to the total dose rate represents the quadratic sum of all known and estimated sources of random and systematic error. No allowance was made for possible biases such as those associated with time-dependent changes in dose rate.

Gamma ray dose rates

There has been some concern about the validity of laboratory measurements to estimate the dose rate for the clearly inhomogeneous PP13B archaeological sediments. This concern relates to estimation of gamma dose rates obtained from a ~40 cm diameter sphere around the sample location and the beta dose rate from a ~6 mm diameter sphere. In the laboratory, we can only assume that the sample we collected is representative.

In situ gamma spectrometry was not feasible for every sample due to the large size of the probe and the small size of some of the sections. We were, however, able to make a single *in situ* measurement in one part of the Eastern excavation area that is representative of samples 46739–43741, and we did a suite of six measurements in the Western excavation area along the N99 E94.5 lines. The *in situ* gamma spectrometry measurements resulted in gamma-ray dose rates that ranged between 0.50 ± 0.01 and 0.61 ± 0.01 Gy/ka in the Western excavation area. This range is consistent with the 0.53 ± 0.02 to 0.65 ± 0.05 Gy/ka range obtained for the gamma-ray dose rates determined in the laboratory (Table 4). The single *in situ* gamma spectrometry measurement in the Eastern excavation area resulted in a gamma-ray dose rate of 0.45 ± 0.01 Gy/ka. The laboratory estimates range between 0.42 ± 0.02 and 0.57 ± 0.04 Gy/ka (Table 4). Although there is variability in the dose rates within each of the excavation areas, the values seem to fall within a restricted range. The dose rates between the different areas are quite different and, in general, the agreement between field and laboratory estimates is satisfactory. Although *in situ* measurements are preferable and more precise, we remain confident that the inhomogeneous nature of the site will not significantly influence the gamma-ray dose rate received by a sample and that the laboratory-based measurements are adequate for age determination of these samples, providing that the subsample being used is representative. A subsequent set of samples, not presented in this paper, for which we determined the gamma-ray dose rate using a portable gamma spectrometer, resulted in ages that are entirely consistent with the ages presented in this paper.

Beta dose rates

There is no feasible way to obtain an estimate of the beta dose rate for each of the measured individual grains. In the laboratory, an average beta dose rate is obtained and it is assumed that this is representative for every grain measured. This may not be true if the sediments are inhomogeneous on a beta scale (~6 mm in diameter around a grain). In fact, the presence of feldspars, calcite, apatite, gypsum, bioclastic particles, stone artifacts, bone, shell, and other common occurrences in archaeological sediments, including the sediments in PP13B (see Karkanas and Goldberg [2010]), renders the assumption to be false. A procedure for assessing the beta dose rate appropriate for age determination has recently been developed for individual quartz grains (Jacobs et al., 2008b). In summary, the procedure initially involves using the finite mixture model (Roberts et al., 2000) to identify the presence of different D_e components in a sample. If a secondary component consisting of low D_e values is identified, then the minimum age model (Galbraith et al., 1999) is used to determine the minimum D_e value for this component. Its corresponding age is obtained by dividing the minimum D_e value by the dose rate with the beta contribution set to zero; this is true of latter amounts too, assuming that these grains had received no beta dose during the period of burial, as would be the case if they had been surrounded by 2 mm of material with negligible radioactivity (e.g., carbonates). If the age obtained in this way approximates that obtained from the main D_e component and the average beta dose rate, then we inferred that all grains in the sample had been deposited at the same time, but had subsequently experienced a range of beta dose rates. Because the grains in the secondary component had experienced below average beta dose rates, then the grains in the main component must have received above average beta dose rates, as the sum of the pair results in the average (measured) beta dose rate for the bulk sample. To deduce the beta dose rate for the main D_e component requires modeling since this value is not measured directly. We estimated the latter beta dose rate based on the relative proportion of grains assigned (by the finite mixture model) to the main component in each sample, following the procedures detailed in Jacobs et al. (2008b).

If the minor low D_e component for the samples at PP13B is taken as an indication for beta microdosimetry, then the dominant effect appears to be from the regions of low radioactivity in the deposit. The minor D_e components in many, but not all, of the samples are consistent with a reduced beta dose rate appropriate for grains that have received a little or no beta dose from their environment. In practice, the ages derived using this procedure are not radically different from those obtained using the average D_e of the main component divided by the sample average total dose rate; the difference was never greater than the 68% confidence limit on the age of the sample itself. However, it was shown in a controlled

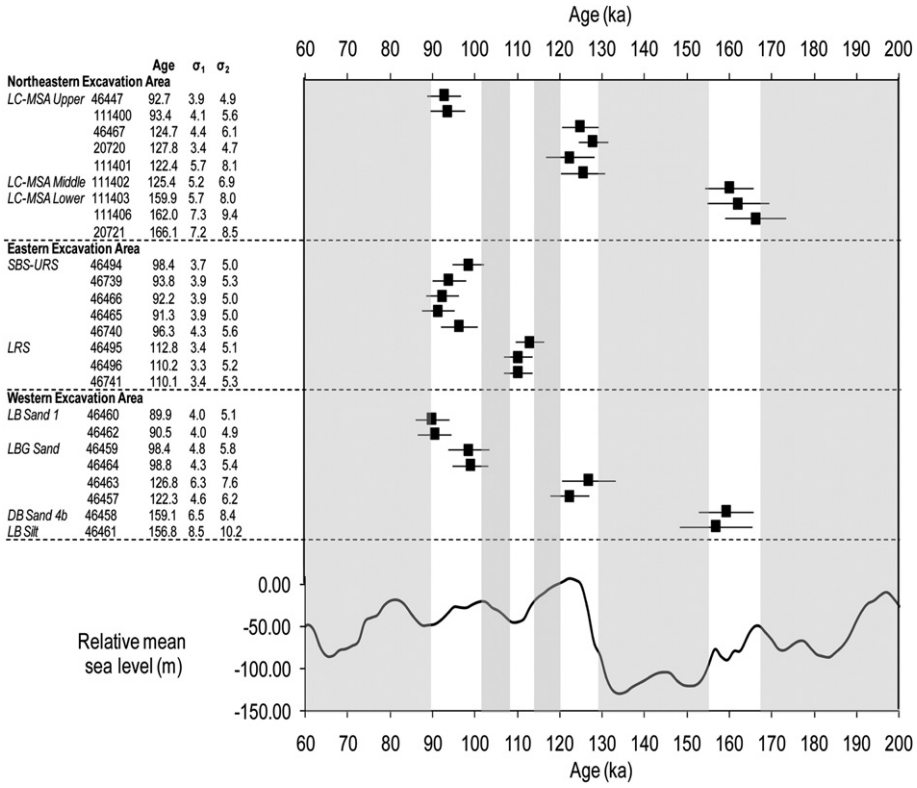

Fig. 4. OSL age estimates (ka) ordered by excavation area and stratigraphic aggregate. Samples are listed in stratigraphic order within each excavation area. The three samples that are >200 ka and the single sample <60 ka are not presented. Standard errors σ_1 and σ_2 exclude and include, respectively, possible systematic error. Each solid square denotes the calculated OSL age and the error bars represent the 68% confidence interval, calculated using σ_1. The gray shading represents those periods during which the site was not occupied, whereas the white shading represents the periods of site occupation. The shading represents the weighted average and σ_1, calculated from the samples that cluster together between all three excavation areas. These periods of site occupation and abandonment are also projected onto the average relative mean sea level curve of Waelbroeck et al. (2002) for the period between 60 and 200 ka.

study by Jacobs et al. (2008b) that the ages derived using the modified dose rate show an overall improvement in reproducibility and stratigraphic consistency and are considered more accurate.

Age calculations

The D_e and dose rate information for all 31 samples are presented in Table 4 and optical ages were estimated by dividing each sample D_e value by its respective total dose rate. The optical ages for 25 samples, excluding the three for which the age is >200 ka, the one with a saturated OSL signal, and 111404 (which is shown in the next section to be an outlier), and their total uncertainties are presented in Figure 4. The total uncertainties (σ_1) associated with the final age determinations include all sources of measured and estimated error in D_e and D_r (Table 4), and the σ_2 error also includes a known possible bias of 3.1% associated with laboratory beta source calibration, beta-counting laboratory standards, and beta dose attenuation. Because these systematic components of variation are common to all samples analyzed in this study, this value is omitted in our statistical comparisons of optical ages within PP13B and with optical ages obtained by Jacobs et al. (2008c); only the random component of variation (σ_1) is relevant in such instances (Aitken, 1985: his Appendix B). The ages obtained for the different excavation areas are discussed below.

Northeastern excavation area

Three of the four ages calculated for the LC-MSA Lower are statistically consistent and a weighted mean age of 162 ± 6 ka was calculated. There is a single outlier (sample 111404), which has a total dose rate 47–54% larger than those of the other three samples from the same unit; hence, we regard its anomalously high dose rate (and correspondingly young optical age) as unreliable.

A single age of 125 ± 5 ka was calculated for the LC-MSA Middle. This is different from the age of 132 ± 6 ka published in Marean et al. (2007) due to the correction that was made for the effects of beta microdosimetry. The OSL ages indicate a depositional break and occupational hiatus lasting 37 ± 6 ka between the LC-MSA Lower and Middle, and this supports the micromorphological observation of an erosional boundary between the two levels (Karkanas and Goldberg, 2010).

No depositional break was observed using sediment micromorphology between the LC-MSA Middle and Upper, and this is supported by the OSL age for the LC-MSA Middle that is consistent with ages obtained for the immediately overlying LC-MSA Upper deposits. These sediments are from an aeolian dune sand that covered the archaeological deposits but did not seal the cave (Lower Dune; Karkanas and Goldberg, 2010; Marean et al., 2010). The three ages are consistent and a weighted mean age of 126 ± 5 ka was calculated. These dune sands are in turn unconformably overlain by another dune sand (Upper Dune) for which a weighted mean age of 93 ± 4 ka was calculated. The optical age for the upper dune sand in LC-MSA Upper is concordant with the U-series age estimate (91.6 ± 1 ka) for the overlying flowstone (Marean et al., 2007, 2010), which provides independent verification of the reliability of the OSL age determinations. The optical ages are also consistent with the coastline model presented by Fisher et al. (2010), which provide further support particularly for

the LC-MSA Lower ages in that the coast was close enough for shellfish gathering only at this time during MIS 6.

The uncertainties associated with the OSL ages for the LC-MSA deposits are due to the very complex depositional and erosional history of this deposit that has also clearly undergone some geochemical changes (i.e., post-depositional cementation of the deposits; Karkanas and Goldberg, 2010). These factors complicate the calculation of the environmental dose rate. The uncertainties in dose rate combined with the evidence for root activity makes the dating of this deposit very challenging. But, the stratigraphic consistency, the reproducibility of ages for samples from the same stratigraphic units, and the concordance with the U-series ages and observations with sediment micromorphology suggest that the ages are meaningful. The ages for this deposit should, however, be considered within the limits of their 95% confidence bounds.

Eastern excavation area

The two ages for the LRS facies (46496 and 46741) are statistically consistent. A weighted mean age of 110 ± 4 ka was calculated. The ages for the SBS-URS facies show similar consistency (except for sample 46495) and there is no difference in the age of SBS and URS where samples could be assigned to one or the other. This is true for samples that are laterally disjointed and spatially removed by at least 2 m. A weighted mean age for this facies of 94 ± 3 ka was calculated. The age for sample 46495 (113 ± 5 ka) is consistent with the weighted mean age for the LRS. Since the total dose rate for all three samples taken from the same profile are very similar (samples 46494–46496; see SOM Fig. 3 and Table 4), and the D_e values from this sample and the underlying LRS sample (46496) are almost identical, it is likely that this sample may actually be from the LRS, rather than the URS. If this age is included in the weighted mean estimate for the LRS then that becomes 111 ± 4 ka, and it is likely that there was a break in occupation between the LRS and SBS-URS that lasted 16.6 ± 2.6 thousand years. The archaeological assemblage from the LRS is, however, very small ($n = 42$; Thompson et al., 2010). The D_e distributions do not suggest any evidence for post-depositional mixing between the LRS and URS, so it is unlikely that these few artifacts percolated down into the underlying units and it is, therefore, believed that they do represent two discrete periods of occupation. The SBS-URS probably represent the final occupation of PP13B prior to the formation of the large dune that sealed the cave at 93 ± 4 ka (LC-MSA Upper) as recorded in the Northeastern excavation area.

Western excavation area

The ages for the three samples from the laminated facies at the base of the excavation have a weighted mean age estimate of 385 ± 17 ka (Table 4). This indicates deposition of the sediments immediately after the MIS 11 high sea level at ~400 ka. We can, on the basis of these ages surmise that the boulders at the base represent deposition during the MIS 11 high sea level. These MIS 11 ages also agree with the micromorphology and geological interpretations that suggest that the cave configuration at this time was different, the groundwater table was higher, sea level was higher, and the land surface was elevated (Karkanas and Goldberg, 2010). No age has yet been determined for the base of the LB Silt facies as the OSL signal for the sample taken from it was in saturation, but the top of LB Silt was estimated to be 157 ± 10 ka (46461). This represents a significant break in sediment deposition in PP13B with a duration of 228 ± 15 thousand years and, again, concurs with micromorphological observations which identified a significant erosion of sediment subsequent to the formation of the laminated facies (Karkanas and Goldberg, 2010). Although there are some lithic materials and bone found within the laminated facies and LB Silt facies, those units are generally regarded as archaeologically sterile and the first evidence for occupation in the Western excavation area occurs in the DB Sand 4 units. A single-age estimate of 159 ± 8 ka was obtained for DB Sand 4b (46458). This is indistinguishable from the age obtained for the top of LB Silt, near the base of LBG Sand 3 (46461). Four further age estimates were obtained for the LBG Sand stratified between the DB Sand 4 and DB Sand 3 units. This LBG Sand is the thickest and laterally most extensive layer in the Western excavation area, but is also disturbed in several areas by subsidence and slumping (Marean et al., 2010). Two age clusters were obtained from the LBG Sand 1 unit—a weighted mean age estimate of 124 ± 5 ka for samples 46457 and 46463 and a weighted mean age estimate of 99 ± 4 ka for samples 46459 and 46464. Based on the age estimates, a sedimentary break of 25 ± 5 ka seems to be present, but this was not detected stratigraphically. However, the latter two samples were collected from sediments where the contact with the overlying DB Sand 3 unit was diffused, whereas the former two samples were collected from sediments where the contact with the overlying DB Sand 3 unit was very sharp. This means that either the younger sand was truncated off in the areas where the contact was sharp (truncations are common in this area) or the top part of the sands were remobilized through trampling or other anthropogenic or geomorphological processes and re-exposed to sunlight, which would have reset the luminescence signal. The former seems more likely than the latter within the broader context of the stratigraphy of this area. No OSL ages were obtained from the archaeologically rich DB Sand 3, but it is bracketed by OSL ages from the underlying LBG Sand (99 ± 4 ka) and the overlying LB Sand 1 for which a weighted mean age of 90 ± 4 ka was calculated.

Discussion and conclusions

Changes in sea level and the input of sand, possibly as a result of the changes in sea level, have played a major role in the formation and preservation of the archaeological deposits in PP13B. The marine-aeolian-anthropogenic connection is evident in both the geological and archaeological history of the site. Being located on a fairly shallow and broad continental shelf further exaggerates this relationship, resulting in PP13B being a coastal site at periods of high sea level and a more terrestrial locality during periods of low sea level (Fig. 4). From the point of view of human occupation, perhaps it was less ideal as a terrestrial locality, being far removed from fresh water sources and the constant food source that the ocean can provide. The age of the laminated facies at the back of the cave, overlying a boulder bed, suggests that PP13B has been available as a living space for at least the last 400 ka (MIS 11).

The first evidence for human occupation in PP13B occurs in both the LC-MSA Lower (Northeastern excavation area) and the DB Sand 4b deposits in the Western excavation area. A weighted mean age estimate of 162 ± 5 ka can be calculated for the deposits from both parts of the cave. This age overlaps at one standard error with a short-duration rise in sea level during MIS 6, about 167 ka ago, which would have brought the coast to within 10 km from the cave site (see Fig. 4). Marean et al. (2007) suggested that this is significant in the light of the existence of marine shells within the deposit. People rarely ventured further than 10 km from the coast to procure and consume seafood. The cave then appears to be abandoned, until evidence for occupation occurred again ~125 ka ago during MIS 5e in both the LC-MSA Middle and Upper in the Northeastern excavation area and in the Western excavation area at the base of LBG Sand 1. Evidence for occupation is very dense within the LC-MSA Middle, but in the LC-MSA Upper and LBG Sand 1 lithic materials and fauna (bone and shell) only occur in low

frequencies throughout the sediments. The sediments are very sandy, suggesting that the shore was very close and sand dunes were present around the cave. The exact sequence of events is not clear from the dating of the deposits at PP13B (Fig. 4). For example, it is unclear whether the occupation in LC-MSA Middle and Upper and LBG Sand 1 occurred before or after the MIS 5e high sea level stand where sea levels were ~5–6 m higher than mean sea level today (Fig. 4). Evidence for this highstand in the form of beach rocks, tidal inlet facies, and sandy shoreface facies along the Cape coast is quite common, but chronologically still poorly constrained. OSL ages have been obtained for such marginal marine facies at four locations along the coast, at Nahoon in the Eastern Cape (Jacobs and Roberts, 2009c), and also closer to PP13B at Sedgefield, Great Brak River, and Agulhas (Carr et al., 2010). These ages range between 138 ± 7 and 117 ± 6 ka and are all statistically consistent with each other, and when combined, they result in a weighted mean age estimate of 126 ± 3 ka. This weighted mean age estimate is consistent with independent estimates of 126 ± 1.7 ka (based on a compilation of U-series ages) for the MIS 5e maximum (Waelbroeck et al., 2008). At these sites, aeolianites conformably overlie the marine facies, and ages obtained for these aeolianites range between 113 ± 6 and 122 ± 7 ka, which suggests a marine–aeolian association. At Nahoon, aeolianites are also found underneath the dated beach rock and have ages of 122 ± 6 and 125 ± 5 ka. This sequence at Nahoon is consistent with some oxygen isotope curves that suggest two sea level highstands during the MIS 5e substage (Kukla et al., 1997; Shackleton, 2000). In the immediate vicinity of PP13B at another cave site, Crevice Cave, aeolianites with ages centered on 127 ± 3 ka have also been dated (Bar-Matthews et al., 2010). Although it is not possible to conclusively determine the sequence of events, it appears as if the occupation may have been slightly before or at the same time as the sea-level highstand, rather than contemporary with the aeolian activity subsequent to the highstand that is recorded at a slightly later age elsewhere in the area (e.g., Carr et al. 2010). It may be that some of the deposits were eroded away as a result of sea spray and other processes associated with the high sea level during MIS 5e.

The next phase of occupation occurred at ~110 ka. This was only evident from the very sparse archaeological remains found in the Lower Roof Spall (LRS) facies in the Eastern excavation area. Only 42 artifacts were recovered from this stratigraphic aggregate, but they were sufficiently different from the artifacts in the units overlying them to dismiss possible downward intrusion of artifacts (Thompson et al., 2010). The densest occupation horizon at PP13B occurs in DB Sand 3. There are no direct ages for this layer, but we obtained ages from samples that clearly bracket these deposits. The top of the underlying LBG Sand 1 was dated to 99 ± 4 ka and the overlying LB Sand 1 (which also contains evidence of occupation) to 90 ± 4 ka. This suggests that the occupation occurred sometime between 100 and 90 ka ago. Further evidence for occupation at this time was also found in the SBS-URS units in the Eastern excavation for which a weighted mean age estimate of 94 ± 3 ka was calculated. Thompson et al. (2010) suggest that the artifacts extracted from these ~95 ka old sedimentary deposits in both excavation areas are in many ways similar to the MSA 2b deposits at Klasies River main site (KR). The MSA 2b deposits at KR have been dated to between 95 and 100 ka based on U-series dating of the bases of two speleothems that formed on top of Layer 14 in the SAS Member (Vogel, 2001). These U-series ages are consistent with the ages determined for the sediments from PP13B and similar to the age obtained for the BBC M3 deposits in Blombos Cave, dated to ~99 ka (Jacobs et al., 2006c). Thus, MIS 5c (99–91 ka) seems to have been a favorable period of occupation along the southern and eastern coasts of South Africa.

The final chapter in the depositional history of the cave site is represented by a second and more substantial dune, which backed up against the cliff and deposited a capping sand layer during the transition from MIS 5c to MIS 5b. This dune was dated at the front of the cave in the LC-MSA Upper to 93 ± 4 ka and is overlain by a flowstone that has a basal age of 91 ± 1.7 ka. This flowstone formation sealed the sand dune and also the cave and prevented further human occupation until 39 ka when it stopped forming. Evidence for this dune was also found inside Crevice Cave and along the cliff face above Crevice Cave where a weighted mean OSL age estimate of 90 ± 2 ka was obtained for four samples (Bar-Matthews et al., 2010).

In conclusion, based on the OSL chronology of the site, there appears to be quite a good relationship between the deposits excavated in the three different excavation areas (see Fig. 4). Although the stratigraphy is complicated by several erosional and cutting events, the general sequence of events appears to have been preserved at the site. This allows an improved understanding of this intricate interplay between dune formation, fluctuating sea levels, and human populations living in the coastal environment. It also provides insights into when these cave sites had been occupied and why archaeological materials have been preserved. For example, at both PP13B and at Blombos Cave, dunes sealed the caves at different times for considerable durations (many tens of thousands of years), making the sites unavailable as living spaces for humans (Jacobs et al., 2003a, 2006c; Marean et al., 2007, 2010), which also explains some of the considerable occupational hiati that can be observed in the archaeological record. The PP13B OSL chronology now extends the common timescale of Jacobs et al. (2008c) for the MSA of Southern Africa to ~170 ka and forms the basis for further age determinations at sites with similar archaeological deposits. This will aid future studies aimed at improving the estimation of the start and end ages of different lithic industries and the fine-tuning of the link between human occupation, dispersal, and environmental change.

Acknowledgements

The majority of this research was funded by the National Science Foundation (USA; grants # BCS-9912465, BCS-0130713, and BCS-0524087 to Marean) and the Australian Research Council through Discovery Project grant DP0666084 to Jacobs. I would like to thank Erich Fisher for producing Figure 1 and SOM Figures 1–9, and the anonymous referees for constructive criticism of the paper.

Appendix. Supplementary data

Supplementary data associated with this article can be found in the online version, at doi:10.1016/j.jhevol.2010.07.010.

References

Adamiec, G., Aitken, M.J., 1998. Dose-rate conversion factors: update. Ancient TL 16, 37–49.
Adamiec, G., Bailey, R.M., Wang, X.L., Wintle, A.G., 2008. The mechanism of thermally transferred optically stimulated luminescence in quartz. J. Phys. D Appl. Phys. 41, 135503.
Aitken, M.J., 1985. Thermoluminescence Dating. Academic Press, London.
Aitken, M.J., 1998. An Introduction to Optical Dating. Oxford University Press, Oxford.
Bar-Matthews, M., Marean, C.W., Jacobs, Z., Karkanas, P., Fisher, E.C., Herries, A.I.R., Brown, K., Williams, H.M., Bernatchez, J., Ayalon, A., Nilssen, P.J., 2010. A high resolution and continuous isotopic speleothem record of paleoclimate and paleoenvironment from 90–53 ka from Pinnacle Point on the south coast of South Africa. Quatern. Sci. Rev. 29, 2131–2145.
Bell, W.T., Zimmerman, D.W., 1978. The effect of HF etching on the morphology of quartz inclusions for thermoluminescence dating. Archaeometry 20, 63–65.
Bernatchez, J.A., 2010. Taphonomic implications of orientation of plotted finds from Pinnacle Point Cave 13B (Mossel Bay, Western Cape Province, South Africa). J. Hum. Evol. 59 (3–4), 247–288.
Bird, M.I., Fifield, L.K., Santos, G.M., Beaumont, P.B., Zhou, Y., di Tada, M.L., Hausladen, P.A., 2003. Radiocarbon dating from 40 to 60 ka BP at Border Cave, South Africa. Quatern. Sci. Rev. 22, 943–947.

Bøtter-Jensen, L., Bulur, E., Duller, G.A.T., Murray, A.S., 2000. Advances in luminescence instruments systems. Rad. Meas. 32, 523–528.
Bøtter-Jensen, L., Mejdahl, V., 1988. Assessment of beta dose-rate using a GM multicounter system. Nucl. Tracks Rad. Meas. 14, 187–191.
Bøtter-Jensen, L., McKeever, S.W.S., Wintle, A.G., 2003. Optically Stimulated Luminescence Dosimetry. Elsevier, Amsterdam.
Carr, A.S., Bateman, M.D., Holmes, P.J., 2007. Developing a 150 ka luminescence chronology for the barrier dunes of the southern Cape, South Africa. Quatern. Geochronol. 2, 110–116.
Carr, A.S., Bateman, M.D., Roberts, D.L., Murray-Wallace, C.V., Jacobs, Z., Holmes, P.J., 2010. The last interglacial sea-level high stand on the southern Cape coastline of South Africa. Quatern. Res. 73, 351–363.
Chen, G., Murray, A.S., Li, S.-H., 2001. Effect of heating on the quartz dose-response curve. Rad. Meas. 33, 59–63.
Clark, J.L., Plug, I., 2008. Animal exploitation strategies during the South African Middle Stone Age: Howiesons Poort and post-Howiesons Poort fauna from Sibudu Cave. J. Hum. Evol. 54, 886–898.
David, B., Roberts, R.G., Magee, J., Mialanes, J., Turney, C., Bird, M., White, C., Fifield, L.K., Tibby, J., 2007. Sediment mixing at Nonda Rock: investigations of stratigraphic integrity at an early archaeological site in northern Australia and implications for the human colonisation of the continent. J. Quatern. Sci. 22, 449–479.
d'Errico, F., Henshilwood, C.S., 2007. Additional evidence for bone technology in the southern African Middle Stone Age. J. Hum. Evol. 52, 142–163.
Duller, G.A.T., 2004. Luminescence dating of Quaternary sediment: recent developments. J. Quatern. Sci. 19, 183–192.
Duller, G.A.T., 2007. Assessing the error on equivalent dose estimates derived from single aliquot regenerative dose measurements. Ancient TL 25, 15–24.
Duller, G.A.T., 2008. Single-grain optical dating of Quaternary sediments: why aliquot size matters in luminescence dating. Boreas 37, 589–612.
Feathers, J.K., 2002. Luminescence dating in less than ideal conditions: case studies from Klasies River main site and Duinefontein, South Africa. J. Archaeol. Sci. 29, 177–194.
Feathers, J.K., Holliday, V.T., Meltzer, D.T., 2006. Optically stimulated luminescence dating of Southern high plains archaeological sites. J. Archaeol. Sci. 33, 1651–1665.
Fisher, E.C., Bar-Matthews, M., Jerardino, A., Marean, C.W., 2010. Middle and late Pleistocene paleoscape modeling along the southern Cape coast of South Africa. Quatern. Sci. Rev. 29, 1382–1398.
Galbraith, R.F., 1988. Graphical display of estimates having differing standard errors. Technometrics 30, 271–281.
Galbraith, R.F., 1990. The radial plot: graphical assessment of spread in ages. Nucl. Tracks Rad. Meas. 17, 207–214.
Galbraith, R.F., 2005. Statistics for Fission Track Analysis. Chapman and Hall, London.
Galbraith, R.F., Roberts, R.G., Laslett, G.M., Yoshida, H., Olley, J.M., 1999. Optical dating of single and multiple grains of quartz from Jinmium rock shelter, northern Australia: Part I, experimental design and statistical models. Archaeometry 41, 339–364.
Galbraith, R.F., Roberts, R.G., Yoshida, H., 2005. Error variation in OSL palaeodose estimates from single aliquots of quartz: a factorial experiment. Rad. Meas. 39, 289–307.
Goldberg, P., Miller, C.E., Schiegl, S., Ligouis, B., Berna, F., Conard, N.J., Wadley, L., 2009. Bedding, hearths, and site maintenance in the Middle Stone Age of Sibudu Cave, KwaZulu-Natal, South Africa. Archaeol. Anthropol. Sci. 1, 95–122.
Grün, R., Beaumont, P., 2001. Border Cave revisited: a revised ESR chronology. J. Hum. Evol. 40, 467–482.
Herries, A.I.R., Fisher, E.C., 2010. Multidimensional modelling of magnetic mineralogy as a proxy for fire use and spatial patterning: evidence from the Middle Stone Age sea cave site of Pinnacle Point 13B (Western Cape, South Africa). J. Hum. Evol. 59 (3–4), 306–320.
Jacobs, Z., 2005. Testing and demonstrating the stratigraphic integrity of artefacts from MSA deposits at Blombos Cave, South Africa. In: d'Errico, F., Backwell, L. (Eds.), From Tools to Symbols. From Early Hominids to Modern Humans. Wits University Press, Johannesburg.
Jacobs, Z., Wintle, A.G., Duller, G.A.T., 2003a. Optical dating of dune sand from Blombos Cave, South Africa: I — Multiple grain data. J. Hum. Evol. 44, 599–612.
Jacobs, Z., Duller, G.A.T., Wintle, A.G., 2003b. Optical dating of dune sand from Blombos Cave, South Africa: II—Single grain data. J. Hum. Evol. 44, 613–625.
Jacobs, Z., Duller, G.A.T., Wintle, A.G., 2006a. Interpretation of single grain D_e distributions and calculation of D_e. Rad. Meas. 41, 264–277.
Jacobs, Z., Wintle, A.G., Duller, G.A.T., 2006b. Evaluation of SAR procedures for D_e determination using single aliquots of quartz from two archaeological sites in South Africa. Rad. Meas. 41, 520–533.
Jacobs, Z., Duller, G.A.T., Wintle, A.G., Henshilwood, C.S., 2006c. Extending the chronology of deposits at Blombos Cave, South Africa, back to 140 ka using optical dating of single and multiple grains of quartz. J. Hum. Evol. 51, 255–273.
Jacobs, Z., Roberts, R.G., 2007. Advances in optically stimulated luminescence dating of individual grains of quartz from archaeological deposits. Evol. Anthropol. 16, 210–223.
Jacobs, Z., Roberts, R.G., 2008. Testing times: old and new chronologies for the Howieson's Poort and Still Bay industries in environmental context. S. Afr. Archaeol. Soc. Goodwin Ser. 10, 9–34.
Jacobs, Z., Roberts, R.G., 2009a. Catalysts for Stone Age innovations. Comm. Integ. Biol. 2, 1–4.
Jacobs, Z., Roberts, R.G., 2009b. Human history written in stone and blood. Am. Sci. 97, 302–309.
Jacobs, Z., Roberts, D.L., 2009c. Last interglacial age for aeolian and marine deposits and the Nahoon fossil human footprints, southeast coast of South Africa. Quatern. Geochronol. 4, 160–169.
Jacobs, Z., Wintle, A.G., Duller, G.A.T., Roberts, R.G., Wadley, L., 2008a. New ages for the post-Howiesons Poort, late and final Middle Stone Age at Sibudu, South Africa. J. Archaeol. Sci. 35, 1790–1807.
Jacobs, Z., Wintle, A.G., Roberts, R.G., Duller, G.A.T., 2008b. Equivalent dose distributions from single grains of quartz at Sibudu, South Africa: context, causes and consequences for optical dating of archaeological deposits. J. Archaeol. Sci. 35, 1808–1820.
Jacobs, Z., Roberts, R.G., Galbraith, R., Deacon, H.J., Grün, R., Mackay, A., Mitchell, P., Vogelsang, R., Wadley, L., 2008c. Ages for the Middle Stone Age of southern Africa: implications for human behavior and dispersal. Science 322, 733–735.
Karkanas, P., Goldberg, P., 2010. Site formation processes in site PP13B (Pinnacle Point, South Africa): resolving stratigraphic and depositional complexities with micromorphology. J. Hum. Evol. 59 (3–4), 256–273.
Kukla, G., McManus, J.F., Rousseau, D.-D., Chuine, I., 1997. How long and stable was the Last Interglacial? Quatern. Sci. Rev. 16, 605–612.
Lombard, M., 2007. Evidence for change in Middle Stone Age hunting behaviour at Blombos Cave: results of a macrofracture analysis. S. Afr. Archaeol. Bull. 62, 62–67.
Marean, C.W., Bar-Matthews, M., Bernatchez, J., Fischer, E., Goldberg, P., Herries, A.I.R., Jacobs, Z., Jerardino, A., Karkanas, P., Minichillo, T., Nilssen, P.J., Thompson, E., Watts, I., Williams, H.M., 2007. Early human use of marine resources and pigment in South Africa during the Middle Pleistocene. Nature 449, 905–908.
Marean, C.W., Bar-Matthews, M., Fisher, E., Goldberg, P., Herries, A., Karkanas, P., Nilssen, P.J., Thompson, E., 2010. The stratigraphy of the Middle Stone Age sediments at Pinnacle Point Cave 13B (Mossel Bay, Western Cape Province, South Africa). J. Hum. Evol. 58.
Mejdahl, V., 1979. Thermoluminescence dating: beta-dose attenuation in quartz grains. Archaeometry 21, 61–72.
Miller, G.H., Beaumont, P.B., Deacon, H.J., Brooks, A.S., Hare, P.E., Jull, A.J.T., 1999. Earliest modern humans in southern Africa dated by isoleucine epimerization in ostrich eggshell. Quatern. Sci. Rev. 18, 1537–1548.
Murray, A.S., Roberts, R.G., 1997. Determining the burial time of single grains of quartz using optically stimulated luminescence. Earth Planet Sci. Lett. 152, 163–180.
Murray, A.S., Wintle, A.G., 2000. Luminescence dating of quartz using an improved single-aliquot regenerative-dose protocol. Rad. Meas. 32, 57–73.
Olley, J.M., Pietsch, T., Roberts, R.G., 2004. Optical dating of Holocene sediments from a variety of geomorphic setting using single grains of quartz. Geomorphology 60, 337–358.
Olley, J.M., Roberts, R.G., Murray, A.S., 1997. Disequilibria in the uranium decay series in sedimentary deposits at Allen's Cave, Nullarbor Plain, Australia: implications for dose rate determinations. Rad. Meas. 27, 433–443.
Opperman, H., Heydenrych, B., 1990. A 22 000 year old Stone Age camp site with plant food remains from the North-Eastern Cape. S. Afr. Archaeol. Bull. 45, 93–99.
Pagonis, V., Wintle, A.G., Chen, R., Wang, X.L., 2008. A theoretical model for a new dating protocol for quartz based on thermally transferred OSL (TT-OSL). Rad. Meas. 43, 704–708.
Porat, N., Rosen, S.A., Boaretto, E., Avni, Y., 2006. Dating the Ramat Saharonim late Neolithic desert cult site. J. Archaeol. Sci. 33, 1341–1355.
Prescott, J.R., Hutton, J.T., 1994. Cosmic ray contributions to dose rates for luminescence and ESR dating: large depths and long-term time variations. Rad. Meas. 23, 497–500.
Roberts, R.G., Bird, M., Olley, J., Galbraith, R., Lawson, E., Laslett, G., Yoshida, H., Jones, R., Fullagar, R., Jacobsen, G., Hua, Q., 1998. Optical and radiocarbon dating at Jinmium rock shelter in northern Australia. Nature 393, 358–362.
Roberts, R.G., Galbraith, R.F., Olley, J.M., Yoshida, H., Laslett, G.M., 1999. Optical dating of single and multiple grains of quartz from Jinmium rock shelter, northern Australia: part II, results and implications. Archaeometry 41, 365–395.
Roberts, R.G., Galbraith, R.F., Yoshida, H., Laslett, G.M., Olley, J.M., 2000. Distinguishing dose populations in sediment mixtures: a test of single-grain optical dating procedures using mixtures of laboratory-dosed quartz. Rad. Meas. 32, 459–465.
Shackleton, N.J., 2000. The 100,000-year ice-age cycle identified and found to lag temperature, carbon dioxide and orbital eccentricity. Science 289, 1897–1901.
Smith, M.A., Prescott, J.R., Head, M.J., 1997. Comparison of ^{14}C and luminescence chronologies at Puritjarra rock shelter, central Australia. Quatern. Sci. Rev. 16, 299–320.
Soriano, S., Villa, P., Wadley, L., 2007. Blade technology and tool forms in the Middle Stone Age of South Africa: the Howiesons Poort and post-Howiesons Poort at Rose Cottage Cave. J. Archaeol. Sci. 34, 681–703.
Thompson, E.N., Williams, H.N., Minichillo, T., 2010. Middle and Late Pleistocene Middle Stone Age lithic technology from Pinnacle Point 13B (Mossel Bay, Western Cape Province, South Africa). J. Hum. Evol. 59 (3–4), 358–377.
Tribolo, C., Mercier, N., Rasse, M., Soriano, S., Huysecom, E., 2010. Kobo 1 and L'Abri aux Vaches (Mali, West Africa): two case studies for the optical dating of bioturbated sediments. Quatern. Geochronol. 5, 317–323.
Tribolo, C., Mercier, N., Selo, M., Valladas, H., Joron, J.L., Reyss, J.L., Henshilwood, C.S., Sealy, J.C., Yates, R., 2006. TL dating of burnt lithics from Blombos Cave (South Africa): further evidence for the antiquity of modern human behaviour. Archaeometry 48, 341–357.
Tribolo, C., Mercier, N., Valladas, H., Joron, J.L., Guibert, P., Lefrais, Y., Selo, M., Texier, P.-J., Rigaud, J.-P., Porraz, G., Poggenpoel, C., Parkington, J., Texier, J.-P., Lenoble, A., 2009. Thermoluminescence dating of a Stillbay–Howiesons Poort sequence at Diepkloof rock shelter (Western Cape, South Africa). J. Archaeol. Sci. 36, 730–739.

Tsukamoto, S., Duller, G.A.T., Wintle, A.G., 2008. Characteristics of thermally transferred optically stimulated luminescence (TT-OSL) in quartz and its potential for dating sediments. Rad. Meas. 43, 1204–1218.
Villa, P., Soriano, S., Teyssandier, N., Wurz, S., 2010. The Howieson's Poort and MSA III at Klasies River main site Cave 1A. J. Archaeol. Sci. 37, 630–655.
Vogel, J.C., 2001. Radiometric dates for the Middle Stone Age in South Africa. In: Tobias, P.V., Raath, M., Moggi-Cecchi, J., Doyle, G.A. (Eds.), Humanity from African Naissance to Coming Millennia. University of the Witwatersrand Press, Johannesburg, pp. 261–268.
Wadley, L., 2008. The Howieson's Poort industry of Sibudu Cave. S. Afr. Archaeol. Soc. Goodwin 10, 122–132.
Wadley, L., Mohapi, M., 2008. A segment is not a monolith: evidence from the Howiesons Poort of Sibudu, South Africa. J. Archaeol. Sci. 35, 2594–2605.
Waelbroeck, C., Frank, N., Jouzel, J., Parrenin, F., Masson-Delmotte, V., Genty, D., 2008. Transferring radiometric dating of the last interglacial sea level high stand to marine and ice core records. Earth Planet Sci. Lett. 265, 183–194.
Waelbroeck, C., Labeyrie, L., Michel, E., Duplessy, J.C., McManus, J.F., Lambeck, K., Balbon, E., Labracherie, M., 2002. Sea-level and deep water temperature changes derived from benthic foraminifera isotopic records. Quatern. Sci. Rev. 21, 295–305.
Wang, X.L., Wintle, A.G., Lu, Y.C., 2006. Thermally transferred luminescence in fine-grained quartz from Chinese loess: basic observations. Rad. Meas. 41, 649–658.
Wang, X.L., Wintle, A.G., Lu, Y.C., 2007. Testing a single-aliquot protocol for recuperated OSL dating. Rad. Meas. 42, 380–391.
Yoshida, H., Roberts, R.G., Olley, J.M., 2003. Progress towards single-grain optical dating of fossil mud-wasp nests and associated rock art in northern Australia. Quatern. Sci. Rev. 22, 1273–1278.